

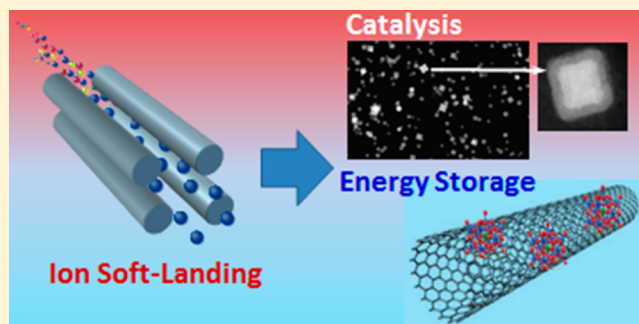
Soft Landing of Complex Ions for Studies in Catalysis and Energy Storage

Julia Laskin,* Grant E. Johnson,* and Venkateshkumar Prabhakaran

Physical Sciences Division, Pacific Northwest National Laboratory, Richland, Washington 99354, United States

ABSTRACT: Immobilization of complex molecules and clusters on supports plays an important role in a variety of disciplines including materials science, catalysis, and biochemistry. In particular, deposition of clusters on surfaces has attracted considerable attention due to their nonscalable and highly size-dependent properties. The ability to precisely control the composition and morphology of complex molecules and clusters on surfaces is crucial for the development of next-generation materials with rationally tailored properties. Soft and reactive landing of ions onto solid or liquid surfaces introduces unprecedented selectivity into surface modification by completely eliminating the effect

of solvent and sample contamination on the quality of the film. The ability to select the mass-to-charge ratio of the precursor ion, its kinetic energy, and charge state along with precise control of the size, shape, and position of the ion beam on the deposition target makes soft landing an attractive approach for surface modification. High-purity uniform thin films on surfaces generated using mass-selected ion deposition facilitate understanding of critical interfacial phenomena relevant to catalysis, energy generation and storage, and materials science. Our efforts have been directed toward understanding charge retention by soft-landed complex ions, which may affect their structure, reactivity, and stability. Specifically, we have examined the effect of the surface on charge retention by both positively and negatively charged ions. We found that the electronic properties of the surface play an important role in charge retention by cations. Meanwhile, the electron binding energy is a key factor determining charge retention by anions. These findings provide the scientific foundation required for the rational design of interfaces for advanced catalysts and energy-storage devices. Further optimization of electrode–electrolyte interfaces for applications in energy storage and electrocatalysis may be achieved by understanding and controlling the properties of soft-landed ions.



1. INTRODUCTION

Nanomaterials play an important role in many areas of research and technology ranging from catalysis,^{1–4} energy conversion and storage,^{5,6} to nanotoxicology⁷ and clinical studies.⁸ Strong dependence of the geometry,^{9,10} electronic structure,^{11,12} and reactivity^{13,14} of metal and metal oxide clusters on their size, charge, and stoichiometry has attracted considerable interest as a means for precisely tailoring the properties of cluster-based materials.¹⁵ Although bare clusters are readily produced using nonthermal gas-phase synthesis approaches,^{16–19} the scalable production of ligated metal clusters in solution provides access to large quantities of cluster-based materials for potential bulk applications.^{20,21} Similarly, polyoxometalates (POMs), a class of stable metal oxide anions prepared through solution-phase condensation of group 5 and 6 transition-metal oxides, have also been widely used as building blocks in materials synthesis^{22–25} due to their diverse optical,²⁶ electrochemical,²⁷ magnetic,²⁸ electro- and photochromic,²⁹ as well as catalytic properties.³⁰ Other complex ions including organometallics have been used as heterogeneous catalysts,^{31–33} photosensitizers,^{33,34} and redox-active materials for energy storage.

Deposition of ions from the gas-phase onto solid and liquid surfaces provides precise control over the size and composition of the supported species, which is critical to understanding

structure–function relationships and the role of ion–support and ion–ion interactions in determining the properties of supported complex ions and their assemblies.^{35–37} Isolated bare metal and metal oxide clusters have been extensively studied both experimentally and theoretically.^{38–46} Gas-phase synthesis of bare metal and metal oxide clusters typically involves the removal of metal from bulk materials using either ion or laser beams or energetic sputtering via plasma–surface interactions, followed by aggregation in a gas condensation region.^{17,18,47} Alternatively, complex ions may be introduced into the gas phase from solution using soft ionization techniques such as electrospray ionization (ESI)⁴⁸ or formed by ESI of metal ions produced using electrochemical oxidation of bulk metal anodes.⁴⁹ Clusters may also be ionized from the solid phase using laser-based approaches such as matrix-assisted laser desorption ionization (MALDI).⁵⁰

Soft landing (SL) of mass-selected ions is ideally suited for deposition of complex ions from the gas phase onto surfaces with precise control of composition, charge state, kinetic energy, and coverage.^{51–56} Furthermore, SL facilitates focusing

Received: June 27, 2016

Revised: August 22, 2016

Published: September 6, 2016

and patterning of the ion beam⁵⁷ along with codeposition of other complex molecules including peptides,^{58,59} proteins,^{60–62} organometallics,^{63–66} and dendrimers,⁶⁷ thereby producing uniform multicomponent films on surfaces with tailored properties. SL has been extensively used for investigating the structure–function relationships of deposited clusters^{3,68,69} and quantifying the effect of the surface on the charge state,^{70–73} structure,⁷⁴ and reactivity⁷⁵ of supported ions. Numerous studies have examined deposition of clusters and complex molecular ions onto self-assembled monolayers (SAMs) and other organic surfaces,^{61,65,70,76–80} metal^{62,81–83} and metal oxide surfaces,^{84–88} and carbon supports (graphite, graphene, carbon nanotubes (CNTs))^{66,89–93} at relatively low coverage (<1 monolayer). The recent development of high-flux ionization sources^{19,94} and ambient SL⁹⁵ has opened up new opportunities for the fabrication of 2D and 3D materials for studies of interfacial phenomena of interest in catalysis and electrochemical energy conversion, storage, and electrochemical sensors.^{96,97} Of particular interest is the effect of surface and mesoscale interactions on the reactivity and stability of supported nanomaterials.⁹⁸ For example, transfer of charge between supports and soft-landed metal, metal oxide,^{88,99} and metal sulfide clusters¹⁰⁰ is a critical phenomenon that has been demonstrated to affect cluster reactivity and stability, especially at the cluster–support interface.^{73,101} This article provides a summary of recent efforts in our group focused on the highly selective deposition of complex ions onto surfaces for studies in catalysis and energy storage using SL. We briefly introduce the specially designed instrumentation used for SL of mass-selected ions, discuss charge retention by soft-landed cations and anions, and provide several recent applications of the use of SL for the controlled deposition of catalytically active species and fabrication of high-performance electrodes for energy storage.

2. RATIONAL DESIGN OF INTERFACES USING ION SOFT LANDING

2.1. Projectile Ion Formation.

Although SL is compatible with a variety of ionization techniques,⁵⁴ sources generating continuous ion beams provide the advantage of higher average ion deposition rates and improved signal stability in comparison with pulsed ion sources.⁵⁴ ESI and magnetron sputtering combined with gas aggregation are two ionization techniques used in our laboratory that generate continuous ion beams and provide access to a broad range of projectile ions. ESI has been widely used for SL of ions present as stable species in solution including peptides,^{58,59,89,102} proteins,^{60,61} organometallic complexes,^{63,64,66,77,103} ligated metal clusters,^{70–72} and POM anions.^{104,105} Meanwhile, magnetron sputtering combined with gas aggregation generates bare metal, metal alloy, and core–shell nanoparticles (NPs).^{18,106–108} Furthermore, by adding a carefully selected reactant gas to the aggregation region, metal oxide,¹⁰⁹ metal sulfide,¹¹⁰ and metal carbide NPs as well as core–shell species may be generated. The following sections provide a brief description of the specialized SL instrumentation developed in our laboratory.

2.1.1. Deposition of Electrospray-Generated Ions.

Numerous instrument configurations have been developed by us and other groups for studying SL of ions produced by ESI under both high vacuum and ambient conditions, many of which are described in recent reviews.^{51–55} Instruments developed in our laboratory for studying SL of ions produced by ESI are shown schematically in Figure 1. Figure 1a depicts an instrument

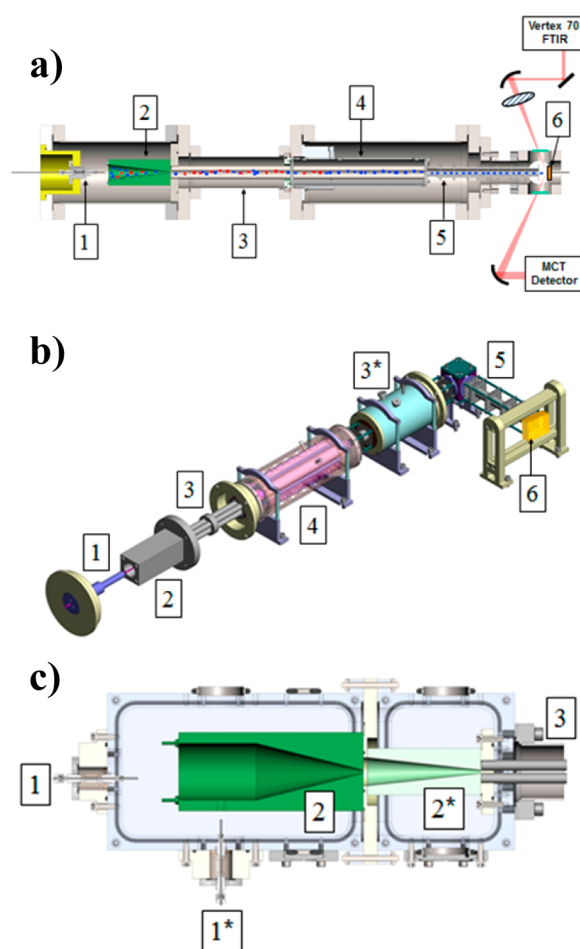


Figure 1. Instruments for studying SL of ions generated by electrospray ionization (ESI): (a) SL instrument configured for in situ IRRAS characterization of surfaces during and after ion deposition; (b) SL instrument coupled to a TOF-SIMS apparatus; (c) a dual ion funnel interface currently coupled to both (a) and (b). The following elements are labeled in the figure: (1, 1*) direct and orthogonal heated inlets, respectively, (2, 2*) ion funnels, (3, 3*) collisional quadrupoles (CQ), (4) RF/DC quadrupole mass filter, (5) electrostatic ion guide, and (6) surface. Adapted with permissions from refs 111, 112, and 94 (© 2015 The Royal Society of Chemistry).

configured for in situ characterization of surfaces using infrared reflection absorption spectroscopy (IRRAS).¹¹¹ In this system, charged droplets produced by ESI are directed into the vacuum system through a heated inlet (1) where they undergo desolvation generating bare ions. Ions are focused by an electrodynamic ion funnel (2) differentially pumped to a pressure of 0.5 to 1 Torr and transferred into a collisional quadrupole (CQ) differentially pumped to 10–50 mTorr (3). Following collisional focusing in the CQ, ions enter a third differentially pumped vacuum chamber equipped with a quadrupole mass filter (4) and electrostatic ion guides (5). Mass-selected ions are focused onto a surface (6) introduced into the vacuum chamber through a vacuum load-lock system. Typical pressure in the third vacuum chamber is in the range of $(2–10) \times 10^{-5}$ Torr during deposition. In the system shown in Figure 1a, the surface is positioned at the focal point of the infrared beam generated by a Bruker Vertex 70 Fourier transform infrared (FTIR) spectrometer (Bruker Optics, Billerica, MA) equipped with a liquid-nitrogen-cooled mercury–cadmium–telluride (MCT) detector. The infrared

beam is focused and directed at the surface at an incidence angle of $\sim 80^\circ$ with respect to the surface normal using one flat and one parabolic gold-coated mirror. A mid-infrared (MIR) KRS-5 wire grid polarizer is used to select p-polarized light known to generate infrared signatures of substrates at grazing angles. The reflected beam is focused onto the MCT detector using two additional parabolic mirrors. Two wedged ZnSe vacuum viewports are used to transfer the infrared beam in and out of the vacuum chamber.

Another custom-built SL apparatus coupled to a commercial time-of-flight secondary ion mass spectrometer (TOF-SIMS) is shown schematically in Figure 1b.¹¹² This instrument is also equipped with a heated inlet (1), ion funnel interface (2), CQ (3), and a quadrupole mass filter (4). A second CQ (3*) installed after the RF/DC quadrupole provides efficient focusing of ions exiting the quadrupole mass filter. A series of einzel lenses and an electrostatic bending quadrupole (5) are used to focus and turn the ion beam 90° prior to deposition. Although typical SL experiments are performed with a deposition spot size of 2 to 3 mm in diameter, focusing of the ion beam on the deposition target to a spot with a full width at half-maximum (fwhm) of ~ 0.3 mm with minimal loss of ion current has been demonstrated using a position sensitive pixel-based detector array (IonCCD).^{113,114} Following ion deposition, the surface may be transferred into the TOF-SIMS instrument for characterization.

Typical ion currents obtained using the instrument configurations described above are in the range of 50–250 pA/charge. A substantial increase in ion current by a factor of 5 to 6 has been achieved recently using a dual ion funnel interface shown in Figure 1c.⁹⁴ In this system, the first ion funnel (2) is operated at a higher pressure of 1–10 Torr, while the second ion funnel (2*) is differentially pumped to an operating pressure of 0.4 to 1.5 Torr. Higher pressure in the first ion funnel is achieved using a heated inlet with a larger inner diameter (ID), which also improves the efficiency of ion transfer into the vacuum system. The best performance of the dual-ion funnel system was achieved using a heated inlet with 1.4 mm ID in the orthogonal geometry (1*). In this configuration, a deposition rate of ~ 1 $\mu\text{g}/\text{day}$ was obtained for mass-selected $\text{PMo}_{12}\text{O}_{40}^{3-}$ cluster ions. High deposition rates achievable using SL instruments are critical to the controlled preparation of molecular assemblies and 3D architectures as well as device fabrication, which is discussed later in this article.

2.1.2. Gas-Phase Synthesis and Deposition of Metastable Species. Gas-phase synthesis and SL of metastable species provide access to unique materials that cannot be generated using solution-phase approaches. Metastable species can be produced by either modifying stable ions in the gas phase (top-down approach) or using ion-induced gas phase nucleation of atomic or molecular precursors (bottom up approach). For example, collision-induced dissociation (CID),^{94,115} ion–molecule,¹¹⁶ and ion–ion chemistry¹¹⁷ may be used to modify stable ions produced by ESI or other ionization techniques. The newly formed species are deposited onto surfaces for subsequent characterization of their structure and reactivity. Alternatively, aggregation in the gas phase following laser ablation or sputtering of solid materials may be used to generate a wide range of cluster ions for SL experiments.

2.1.2.1. Gas-Phase Modification of Stable Ions. Gas-phase ion chemistry may be employed for the controlled modification of stable ions produced using ESI and other ionization

techniques. For example, Johnson and Laskin used in-source CID to generate undercoordinated $\text{Ru}(\text{bpy})_2^{2+}$ cations (bpy = 2,2'-bipyridine ligand) from stable $\text{Ru}(\text{bpy})_3^{2+}$ precursors for SL on carboxyl-terminated SAMs (COOH-SAMs) at 50 eV collision energy.⁶³ The COOH-SAM was selected as the substrate because previous studies indicated that an electrostatic bond forms between cations and the anionic carboxylate groups of the monolayer resulting in efficient surface immobilization.⁵⁸ Strong immobilization of $\text{Ru}(\text{bpy})_2^{2+}$ is evidenced by the presence of the thiol-bound $\text{Ru}(\text{bpy})_2(\text{C}_{16}\text{H}_{30}\text{O}_2\text{S})^+$ complex in the TOF-SIMS spectrum shown in Figure 2. Interestingly, the adduct peak exhibits

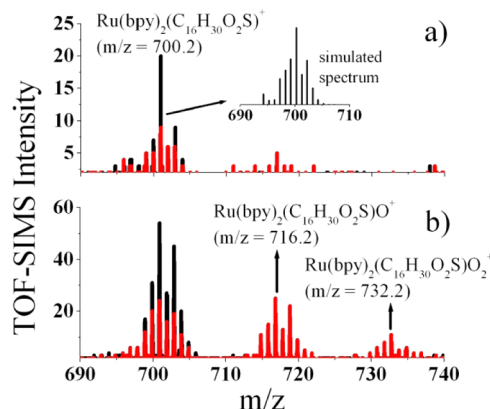


Figure 2. Portion of the TOF-SIMS spectra obtained after SL of mass-selected (a) $\text{Ru}(\text{bpy})_3^{2+}$ and (b) $\text{Ru}(\text{bpy})_2^{2+}$ onto COOH-SAMs. The black spectrum was obtained following SL. The red spectrum was obtained following exposure to O_2 . Adapted with permission from ref 63. © 2010 Wiley-VCH.

substantially larger abundance following SL of an equal amount of $\text{Ru}(\text{bpy})_2^{2+}$ (Figure 2b) compared with $\text{Ru}(\text{bpy})_3^{2+}$ (Figure 2a). We proposed that the reaction of the fully ligated complex with the COOH-SAM involves stripping of one bipyridine ligand through surface-induced dissociation (SID)⁵⁵ at the time of collision followed by electrostatic immobilization of the resulting undercoordinated ions. The fact that a lower abundance of immobilized adduct was observed following SL of fully ligated ions suggests that only a fraction of the $\text{Ru}(\text{bpy})_3^{2+}$ ions had sufficient kinetic energy to undergo dissociation and adduct formation during collision with the surface. In contrast, dissociation of $\text{Ru}(\text{bpy})_3^{2+}$ in the gas phase prior to SL, illustrated in Figure 3a, results in more efficient adduct formation, consistent with the higher reactivity of the undercoordinated species.

The reactivity of immobilized $\text{Ru}(\text{bpy})_2^{2+}$ was examined by sequentially exposing the surface to gaseous reagents (O_2 and C_2H_4).⁶³ The SIMS spectra obtained following exposure to O_2 are presented in red in Figure 2. Oxidation of the complex upon exposure to O_2 results in the formation of the $\text{Ru}(\text{bpy})_2(\text{C}_{16}\text{H}_{30}\text{O}_2\text{S})\text{O}^+$ species. Subsequent reduction following exposure to C_2H_4 regenerates the $\text{Ru}(\text{bpy})_2(\text{C}_{16}\text{H}_{30}\text{O}_2\text{S})^+$ complex. Therefore, the immobilized $\text{Ru}(\text{bpy})_2^{2+}$ complexes exhibit behavior consistent with hydrocarbon oxidation, which is an important catalytic process for commercial chemical production and pollution abatement. The ratios of the integrated abundances of the reduced and oxidized adducts are shown in Figure 3b. The ratios indicate that there is a reproducible increase in the relative abundance of oxidized adduct following exposure of the surface to O_2 and an increase

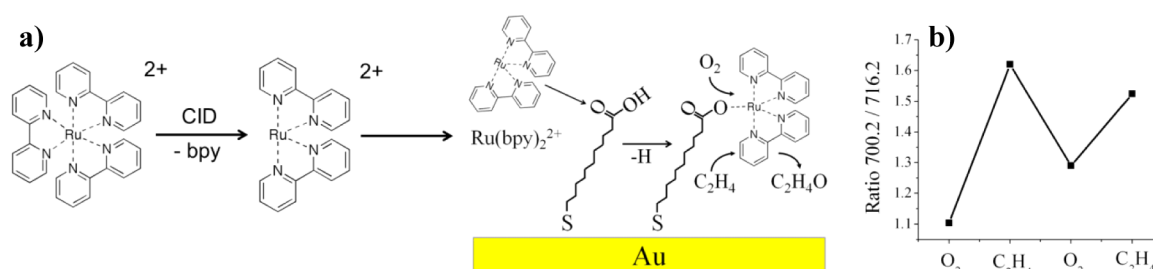


Figure 3. (a) Schematic illustration of the conversion of fully ligated $\text{Ru}(\text{bpy})_3^{2+}$ to undercoordinated $\text{Ru}(\text{bpy})_2^{2+}$ and SL onto COOH-SAMs. (b) Ratio of the TOF-SIMS abundances of $\text{Ru}(\text{bpy})_2(\text{C}_{16}\text{H}_{30}\text{O}_2\text{S})^+$ (m/z 700.2) to $\text{Ru}(\text{bpy})_3(\text{C}_{16}\text{H}_{30}\text{O}_2\text{S})\text{O}^+$ (m/z 716.2) obtained after exposure to O_2 and C_2H_4 showing catalytic activity of $\text{Ru}(\text{bpy})_2^{2+}$. Adapted with permission from ref 63. © 2010 Wiley-VCH.

in the abundance of reduced adduct after exposure to C_2H_4 . In comparison, soft-landed $\text{Ru}(\text{bpy})_3^{2+}$ does not show similar behavior, indicating that through gas-phase ligand stripping it is possible to convert a relatively inert fully ligated organometallic complex into a catalytically active undercoordinated metal center that is immobilized on SAM surfaces through an electrostatic bond. This unique capability of preparative mass spectrometry provides an opportunity to produce novel surface-bound organometallic complexes with partially open coordination spheres that are not obtainable in solution and may exhibit improved performance, stability, and recyclability for applications in catalysis.³²

In a subsequent study, in-source CID of ligated gold clusters generated using reduction synthesis in solution was employed to produce reactive cluster ions for subsequent deposition onto surfaces. Specifically, $\text{Au}_{11}\text{L}_5^{3+}$ ($\text{L} = 1,3$ -bis(diphenylphosphino)propane, DPPP), denoted as $(11,5)^{3+}$, synthesized in solution were introduced into the gas phase using ESI and subjected to in-source CID. The abbreviated bracket notation $(x,y)^z$ designates the number of gold atoms (x), diphosphine ligands (y), and the ionic charge (z) of the cluster. The most abundant fragment of the $(11,5)^{3+}$ cluster, $(10,4)^{2+}$, was mass-selected and soft-landed onto COOH-SAM and SAMs of alkythiol (HSAM) and perfluorinated alkythiol (FSAM). It was demonstrated that the $(10,4)^{2+}$ fragment ions are much more reactive than the stable $(11,5)^{3+}$ precursor clusters. The enhanced reactivity was evidenced by the presence of abundant adducts of the $(10,4)^{2+}$ ion formed during TOF-SIMS analysis. These results indicate that some fragment ions formed by in-source CID of ligated clusters are more prone to reaction on SAM surfaces than cluster ions that are soft-landed intact from solution. This observation is consistent with the coordinative undersaturation of fragment ions that exposes bare metal sites at the cluster surface that may exhibit enhanced reactivity compared with fully ligated species. It follows that SL combined with in-source CID offers a versatile approach for preparing novel active partially ligated clusters that cannot be obtained in solution. Such partially ligated clusters may exhibit enhanced catalytic properties and improved stability toward sintering.^{118,119}

2.1.2.2. Nonthermal Physical Synthesis. Physical synthesis techniques have been developed to prepare bare NPs and clusters without the use of solvents and organic ligands, which can introduce contaminants and often necessitate additional postsynthesis cleaning and ligand removal steps. These gas-phase methods include but are not limited to elemental vapor reaction,¹²⁰ gas condensation,¹²¹ laser vaporization,^{16,17} magnetron sputtering,^{18,122} ion sputtering,¹²³ and pulsed arc synthesis.¹²⁴ Most of these techniques are implemented at

subambient pressures and coupled to electrostatic, electrodynamic, or magnetic mass filters and charged particle optics that allow a predetermined species to be separated from the overall distribution of ions produced by the source. Traditionally, the maximum stable ion currents (over a time scale of hours) produced with these methods were on the order of picoamperes (10^{-12} A) which limited their applications to preparing well-defined species on small area surfaces at low coverage for fundamental research in surface science and catalysis.³⁷ More recently, breakthroughs in ion production,¹²⁵ transmission,⁹⁴ and mass-filtering¹²⁶ have allowed larger ion currents of up to 6 nanoamperes (10^{-9} A) of mass-selected clusters to be delivered to surfaces.³⁶ In addition, a new “matrix assembly cluster source” has been introduced by Palmer and coworkers with the potential for scale up to produce milliamps of current.¹⁹ This substantial increase in deposition rate provides an unparalleled opportunity for SL of mass-selected ions to enter the manufacturing of high-value components including solar cells,¹²⁷ shallow junctions in integrated circuits,¹²⁸ and energy-storage devices.⁹⁶

Direct current (DC) magnetron sputtering from one or several targets coupled to inert gas condensation evolved into a versatile approach for preparing bare NP and cluster ions over a broad range of sizes and compositions that are not accessible using thermal synthesis in solution.^{129–134} This nonequilibrium method does not require ligands or solvent, which surmounts many of the challenges associated with solution-phase synthesis approaches. The distribution of NPs and clusters exiting a magnetron sputtering gas condensation source may be adjusted over a substantial range by tuning the flow rates of sputtering (Ar), carrier (He), and reactant gases (e.g., O_2 , CH_4), the current applied to each target, and the position of the magnetron inside the gas condensation region (condensation length).^{135,136} In addition, the ID of the exit aperture of the gas condensation region and the method used for cooling this region (water¹³⁷ or liquid N_2 ¹⁸) may be changed to steer the NP distribution toward a predetermined size, composition, and morphology. The strength of the magnetic fields of the magnetrons at the surface of the sputtering targets also influences NP size and composition by controlling the plasma density. This parameter may be tuned coarsely by substituting magnets of different strength or finely using metal backing plates with adjustable thickness to control the distance of the target to the magnetron.

A custom-modified commercial magnetron sputtering instrument for SL of bare NPs on surfaces with controlled coverage, size, and morphology is shown schematically in Figure 4.¹⁰⁸ In this instrument, NPs are produced by sputtering of up to three independent targets, followed by inert gas condensation and

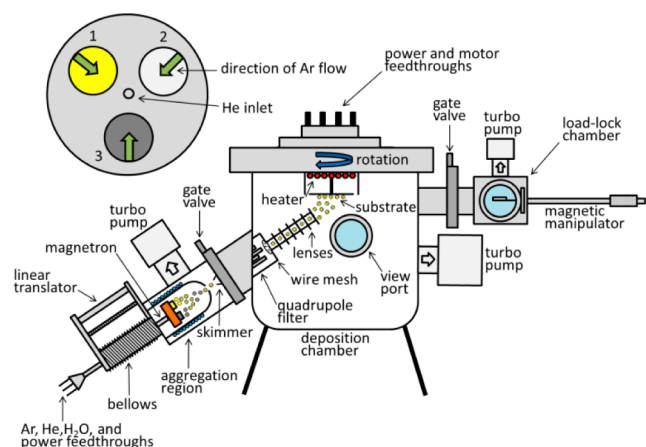


Figure 4. Schematic diagram of the nanocluster deposition system including the Nanogen-Trio nanoparticle source from Mantis Deposition. Note the presence of three separate sputtering targets on the same linear translator within one region of gas aggregation. The insert illustrates the surface of the magnetron head where three targets may be sputtered simultaneously to generate vapors that are swept to the center by Ar gas. Adapted with permission from ref 108. © 2015 Royal Society of Chemistry.

mass selection using a quadrupole mass filter.¹³⁸ The ID of the exit aperture of the gas condensation region was reduced from 5 to 3 mm to facilitate efficient NP formation at lower gas flow rates. In addition, two einzel lenses were mounted in series between the quadrupole mass filter and the deposition target that enabled focusing of the beam of NPs to a circular spot on the surface ~ 2.5 cm in diameter.

Initial experiments explored the influence of different source parameters on single metal (Mo, Ti, and V) as well as bimetallic (Pt/Ti, V/Ti, and Pt/V) NPs that have potential applications in heterogeneous catalysis, fuel cell electrocatalysis, and solar energy conversion.¹³⁹ Utilizing surface characterization techniques including atomic force microscopy (AFM), scanning electron microscopy (SEM), transmission electron microscopy (TEM), and electron energy loss spectroscopy (EELS), the chemical and physical properties of bare size-selected single-metal and bimetallic NPs synthesized using the multitarget magnetron source were investigated. High-angle annular dark-field (HAADF)-STEM images, presented in Figure 5, demonstrated that NPs with spherical or cubic morphology may be formed by controlling the flow rates of Ar and He, thereby supporting the earlier findings reported by Krishnan and coworkers using a related source design.¹⁴⁰ HAADF-STEM imaging also revealed that this physical synthesis approach may be used to prepare NPs with core-shell structures that are desirable for applications in electrocatalysis (Figure 6). Multilayer particles are particularly challenging to synthesize in solution due to the different mixing patterns that may be adopted by the metals and their dissimilar reduction potentials that can lead to particles of single elements clumped together.¹⁴¹ Overall, this study demonstrated that magnetron sputtering and gas condensation is a versatile approach for preparing bare single-metal and alloy NPs on surfaces that are free of the complications resulting from synthesis in solution with solvent and ligands. In addition, because multiple substrates may be mounted simultaneously during deposition, it is possible to characterize how different supports influence the properties of identical NPs prepared at the same time.

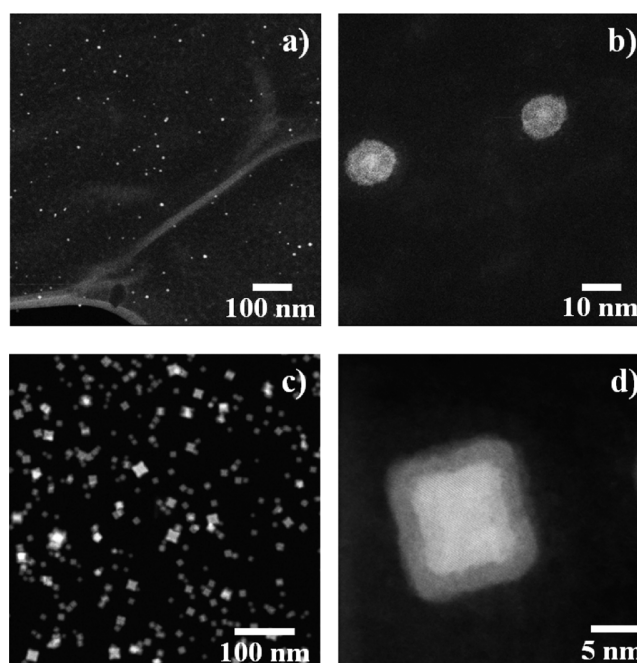


Figure 5. Low (a) and high (b) magnification scanning transmission electron microscopy images obtained for 4×10^4 ions/ μm^2 size-selected anionic 5 nm Mo nanoparticles soft-landed onto a continuous carbon microscopy grid. Low (c) and high (d) magnification images obtained for 2×10^5 ions/ μm^2 size-selected anionic 8 nm V nanoparticles soft-landed onto a carbon grid. Note the monodispersity in size and core-shell structure of the Mo nanoparticles as well as the cubic morphology of the V nanoparticles. Adapted with permission from ref 108. © 2015 Royal Society of Chemistry.

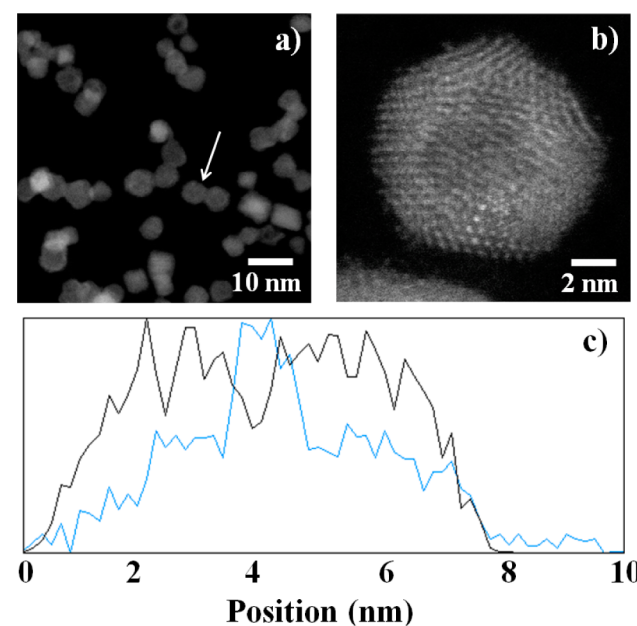


Figure 6. Low (a) and high (b) magnification scanning transmission electron microscopy images obtained for 3×10^5 ions/ μm^2 size-selected anionic 7 nm Pt/V alloy nanoparticles soft-landed onto a continuous carbon microscopy grid. Electron energy loss spectroscopy line profile (c) across a representative nanoparticle. Note the increased Z-contrast of the shell of the nanoparticle and the enrichment of platinum and vanadium at the shell and core, respectively. Adapted with permission from ref 108. © 2015 The Royal Society of Chemistry.

The modified source and deposition instrument were also employed to prepare novel bimetallic PtRu NPs that were subsequently found to be a promising candidate material for promoting the oxygen reduction reaction (ORR), an important electrochemical process that limits the efficiency of proton exchange membrane fuel cells (PEMFCs).^{139,142} Sputtering of two independent Pt and Ru targets coupled to inert gas condensation and SL of mass-selected ions was used to prepare bare PtRu NPs on glassy carbon (GC) electrodes. Employing AFM, it was shown that the NPs bind randomly to the GC electrode at relatively low coverage and that their height distribution is monodisperse and centered at the size selected by the quadrupole filter. High-resolution HAADF-STEM and TEM images further confirmed that the soft-landed PtRu NPs were uniform in size and morphology. Wide-area scans of the coated electrodes using X-ray photoelectron spectroscopy (XPS) revealed the presence of both Pt and Ru in atomic concentrations of ~ 9 and $\sim 33\%$, respectively. Moreover, deconvolution of the high-energy resolution XPS spectra in the Pt 4f and Ru 3d regions indicated the presence of both oxidized Pt and Ru that likely formed upon exposure of the NPs to the ambient environment. The higher loading of Ru compared with Pt and enrichment of Pt at the surface of the NPs was inferred from analysis of the coated electrodes using time-of-flight medium energy ion scattering (TOF-MEIS).

2.2. Effect of Ion-Surface Interactions. Surface properties may exert a pronounced effect on the structure and reactivity of soft-landed ions. Different deposition targets including silicon wafers,¹⁴³ clean and plasma-treated metal surfaces,⁶⁰ carbon electrodes,^{66,89} highly oriented pyrolytic graphite (HOPG),^{90,144} and SAMs^{58,76,145} have been used in SL experiments. The polarizability and presence of charged functional groups on the surface both have a pronounced effect on the binding energy between the soft-landed species and the deposition target.⁵⁹ Relatively weak binding of ions to surfaces may result in desorption of deposited species¹⁰² or substantial diffusion on the surface at room temperature.¹⁴⁶ For example, AFM characterization of V NPs deposited onto GC electrodes revealed the formation of a uniform film of NPs resulting from random binding of soft-landed species to the surface.¹⁰⁸ In contrast, NPs deposited onto HOPG substrates were typically aligned along the step edges, indicating substantial diffusion of NPs due to weaker binding to this surface.¹⁰⁸ Conversely, electrostatic or covalent binding of ions to surfaces may be used for strong immobilization with minimal rearrangement of soft-landed species after collision with a surface. For example, strong binding of $\text{PMo}_{12}\text{O}_{40}^{3-}$ ions to SAMs terminated with charged NH_3^+ groups enabled their characterization using cyclic voltammetry (CV) in an aqueous electrolyte solution.¹⁰⁵ In contrast, $\text{PMo}_{12}\text{O}_{40}^{3-}$ ions soft-landed onto FSAMs were efficiently washed away during the first few CV cycles. It follows that charged surfaces may be used when strong binding of ions is required for a specific application. Meanwhile, weakly binding surfaces may be used to direct assembly of soft-landed species through diffusion. Such assembly may be controlled by tailoring the morphology of the surface¹⁴⁷ and optimizing the binding energy of the soft-landed ions through selective chemical derivatization or physical processing of surfaces using ion beams¹⁴⁸ or plasmas.¹⁴⁹

The binding energy of ions to surfaces is also affected by the charge state of the ion.¹⁵⁰ Since the initial demonstration of charge retention by soft-landed ions by Cooks and coworkers,⁷⁶

substantial effort has been dedicated to understanding this phenomenon.^{70,71,103,105,151,152} SAMs are particularly attractive deposition targets for studying the effect of the surface and properties of the projectile ion on charge retention.^{153,154} In particular, the ability to control the composition, length, and terminal functional group of thiols and their ability to form well-organized nanometer thick insulating films on gold surfaces have prompted systematic studies of charge retention by soft-landed ions on SAMs of thiols on gold.¹⁵⁵ It has been demonstrated that depending on the properties of the surface and the projectile ion, different charge states of the deposited species may be present on the surface. In particular, deprotonation of the soft-landed species is the major charge reduction process observed for protonated molecules on different SAMs.¹⁰² The charge retention efficiency is dependent on the proton affinity of soft-landed protonated molecules⁶⁴ and the properties of the SAM.^{58,152} Specifically, the efficiency decreases in the order FSAM > HSAM > COOH-SAM for protonated peptides with larger species retaining at least one charge on FSAMs.

A different charge reduction mechanism has been observed for native cations soft-landed onto SAMs.^{70,77,103} Specifically, charge reduction by native cations involves electron attachment to the ion and is strongly dependent on the efficiency of electron transfer through the SAM surface, the only source of electrons under high vacuum conditions.^{153,154} The electron tunnelling efficiency of SAMs has been studied using scanning tunneling spectroscopy (STS).¹⁵³ These studies have demonstrated efficient electron tunneling through HSAMs at all applied potentials, less tunneling through COOH-SAMs, and a fairly high barrier to electron transport (~ 1.5 V) through FSAMs which is attributed to the formation of interface dipoles.¹⁵⁴ The observed decrease in the charge retention efficiency of native cations on FSAM > COOH-SAM > HSAM is in excellent agreement with the results of STS studies. Experiments with multiply charged cationic gold clusters also revealed that it is possible to control the charge state of supported clusters through judicious choice of the SAM. For example, $(11,5)^{3+}$ clusters were shown to be present primarily in the 3+, 2+, and 1+ charge states on FSAM, COOH-SAM, and HSAM surfaces, respectively.⁷⁰ Furthermore, studies performed at different coverage revealed that at sufficient loading the potential resulting from the presence of triply charged cations is large enough to overcome the tunnelling barrier on the FSAM, resulting in charge reduction and neutralization of the clusters.⁷¹

In contrast with cations, the properties of the surface play a minor role in determining the charge retention efficiency of soft-landed anions. Specifically, in situ IRRAS in combination with density functional theory (DFT) calculations has been used to examine charge retention by stable multiply charged polyoxometalate (POM) anions, $\text{PM}_{12}\text{O}_{40}^{n-}$ ($M = \text{Mo}, \text{W}; n = 2, 3$), soft-landed onto FSAM, HSAM, and NH_3^+ -SAM surfaces.^{104,105} The results indicate more efficient charge retention by $\text{PW}_{12}\text{O}_{40}$ (WPOM) in comparison with $\text{PMo}_{12}\text{O}_{40}$ (MoPOM).¹⁰⁴ Both clusters undergo partial charge reduction during collision with the surface. For WPOM, slow loss of one electron was observed using time-resolved IRRAS.¹⁰⁴ It has been proposed that the doubly charged WPOM anion is particularly stable on SAM surfaces. In contrast, only a small fraction of MoPOM retains three charges after collision with SAMs.¹⁰⁵ The results obtained for POM anions are consistent with the high barrier for electron

detachment from these species during and after ion-surface collision. For example, the vertical electron detachment energy of MoPOM is 1.94 eV.¹⁵⁶ This value is lower than the value of 2.30 eV reported for WPOM, which is consistent with the more efficient charge retention by WPOM in comparison with MoPOM on the same SAM surface. Our results indicate that the electron affinity of soft-landed anions is the critical factor determining their charge retention properties.

Ionic charge state is an important factor that determines the structure and reactivity of clusters both in the gas phase and on surfaces. For example, Kappes and coworkers demonstrated a charge-state-dependent transition from 2D to 3D structures in Au clusters occurring at 8 gold atoms for cations and 12 gold atoms for anions.¹⁵⁷ The charge state of gas-phase gold and oxide cluster ions has also been shown to influence the CO binding energy^{158,159} and the mechanism of catalytic CO oxidation.^{160,161} Charge-dependent reactivity has been observed for supported metal clusters. For example, the enhanced catalytic activity of Au₈ clusters on MgO surfaces has been attributed to partial transfer of charge to the clusters from the support.⁷³ The charging of supported atoms and clusters may be controlled by tailoring the chemical properties of the surface¹⁶² or by introducing defects or dopant atoms into the support.^{73,163} These surface features exert a sizable influence on the reactivity and stability of supported cluster ensembles.⁵⁴ Surface defects also influence the binding energies of reactants and intermediates to supported clusters, thereby controlling their catalytic reactivity.¹⁶⁴ Furthermore, the oxidation state of the support is known to affect the reactivity of immobilized clusters.¹⁶⁵ The strength of the cluster–support interaction determines whether clusters migrate on the surface and coalesce under reaction conditions.^{166–169} In particular, the driving force for Ostwald ripening, a key degradation process of supported particles during catalytic reactions, is the different chemical potentials of smaller and larger clusters that are present in the same ensemble.¹⁶⁷ A number of approaches, therefore, are available to tune the cluster–support interaction, including charging, which profoundly influences reactivity and stability.

Control of surface coverage using SL provides important information on the influence of cluster–cluster distance on the reactivity of soft-landed cluster ions. For example, electrochemical characterization of carbon electrodes containing known coverages of Pt clusters revealed that the proximity of adjacent Pt clusters on the surface strongly influences the efficiency of catalytic O₂ reduction.⁶⁹ This effect is proposed to originate from the overlap of electrical double layers of neighboring clusters at small interparticle distances.⁶⁹ By controlling the surface coverage, therefore, it is possible to tune the local potential at the interface between the supported clusters that influences the binding energy of reactants and intermediates. Collectively, these findings illustrate that it is extremely important to control the charge state of clusters on supports to obtain superior performance from materials for a number of applications.

3. CURRENT AND FUTURE APPLICATIONS OF ION SOFT LANDING FOR STUDIES IN CATALYSIS AND ENERGY STORAGE

3.1. Catalytic Activity of Bare Clusters. SL of mass-selected ions has been utilized to investigate the size-, composition-, and coverage-dependent properties of both bare and ligated clusters and NPs immobilized on supports.⁸⁵

It has been demonstrated that the structure and reactivity of bare subnanometer clusters may vary substantially with the addition or removal of a single atom.^{97,170,171} Extensive work has been performed on a range of different bare metal clusters and support materials as well as chemical reactions that are of both fundamental and industrial importance. For example, Heiz and coworkers demonstrated that Ni₃₀ clusters are more active toward CO dissociation than other cluster sizes near room temperature.¹⁷² In another investigation, Au₈ soft-landed onto MgO containing oxygen vacancy defects was shown to be the smallest cluster that promotes the catalytic oxidation of CO to CO₂, an important reaction for atmospheric pollution abatement.¹⁷³ Theoretical calculations on the supported Au₈ clusters indicated that partial charge transfer from F-center defects on MgO activates the Au₈ clusters toward dissociation of O₂ and catalytic oxidation of CO to CO₂. In a more recent work, Anderson and coworkers characterized the catalytic properties of Pd clusters soft-landed onto TiO₂. They reported a size-dependent change in CO oxidation activity that was correlated with an evolution in the Pd 3d electron binding energies of the supported clusters measured with XPS.⁸⁶ These representative studies provide experimental evidence of the influence of the size-dependent electronic structure of supported metal clusters on their catalytic activity.

The catalytic selectivity of supported clusters has also been examined using model systems prepared by SL. For example, the oxidation of cyclohexane to CO and CO₂ over Pd clusters pinned on graphite was investigated by Palmer and coworkers, revealing an increase in activity with decreasing cluster size.¹⁷⁴ Vajda and coworkers used SL to prepare Ag clusters on Al₂O₃, which were shown to exhibit low-temperature activity toward the epoxidation of propylene to propylene oxide.¹⁷⁵ Theoretical calculations predicted that oxidized Ag₃ clusters are active toward selective oxidation of propylene due to their open-shell electronic structure. In a related contribution, the same group examined the activity of Au clusters on Al₂O₃ toward the epoxidation of propene.¹⁷⁶ It was shown that the highest selectivity was achieved over Au clusters in reaction gas mixtures containing O₂ and H₂O, thereby avoiding the problematic use of H₂ for this industrially important process. More recently, this group demonstrated that mass-selected silver clusters may be used to control the morphology of the discharge products that form in Li-ion batteries.⁹⁷

Our studies are focused on understanding structure–function relationships in the catalytic activity of alloy and hybrid organic–inorganic NPs toward the ORR, an important catalytic process occurring at the cathode of PEMFC.¹⁷⁷ Previously, Chorkendorff and coworkers reported greatly enhanced activity of PtY alloy NPs toward ORR that was attributed to compressive strain due to their core–shell morphology.¹⁷⁸ We examined the catalytic activity of mass-selected soft-landed PtRu NPs toward the electrochemical reduction of O₂ using CV in acidic electrolyte solutions (0.1 M H₂SO₄ and 0.1 M HClO₄) saturated with Ar or O₂.¹⁴² As shown in Figure 7, in both electrolyte solutions pronounced ORR activity was observed in the O₂-saturated electrolytes that was not evident in the Ar-purged electrolytes. Repeated electrochemical cycling of the electrodes revealed no substantial change in the ORR currents or shape and onset of ORR in the CV curves, indicating high stability of the PtRu NPs supported on GC toward deactivation through dissolution, dealloying, or agglomeration. The reproducibility of the NP synthesis and deposition method was also evaluated by employing the same

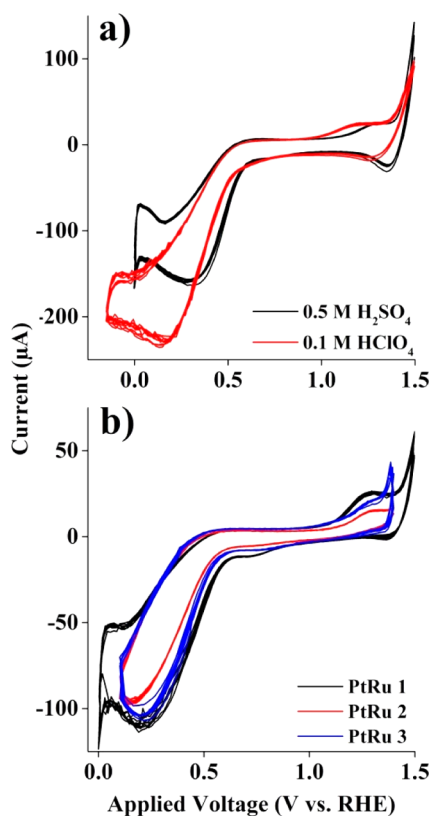


Figure 7. Cyclic voltammograms (a) of 7×10^4 ions μm^{-2} of mass-selected anionic 4.5 nm PtRu nanoparticles soft-landed onto glassy carbon in 0.5 M H_2SO_4 (black line) and 0.1 M HClO_4 (red line) with O_2 purging. Cyclic voltammograms (b) of identical nanoparticles soft-landed on three separate days (black, red, and blue lines) in 0.5 M H_2SO_4 with O_2 purging, scan rate = 100 mV s^{-1} , temperature = 20°C . Adapted with permission from ref 142. © 2015 Royal Society of Chemistry.

instrument parameters on three occasions separated by several days. As shown in Figure 7, electrodes with almost identical electrochemical behavior were observed with CV, demonstrating the reproducible preparation of alloy NPs using the multimagnetron in-plane gas condensation source.

In another study, the potential of reactive magnetron sputtering and gas aggregation as a preparation technique for catalytically active hybrid organic–inorganic NPs was evaluated.¹⁷⁹ Reactive sputtering of Ta in the presence of three model hydrocarbons, 2-butanol, heptane, and *m*-xylene, combined with gas condensation was shown to result in the synthesis of novel NPs. The catalytic activity of the hybrid NPs was evaluated using a GC surface coated with NPs as the working electrode in a three electrode cell. CV curves measured in Ar-saturated electrolyte revealed no additional current compared with the baseline observed for bare GC. In comparison, both the Ta-heptane and Ta-xylene but not the Ta-butanol NPs exhibited large reduction currents consistent with the ORR in the O_2 -saturated electrolyte. Furthermore, the CV curves remained stable following repeated potential cycling, indicating that the NPs are both active and robust. A suite of characterization techniques was employed to investigate how key source parameters including the flow rate of the He carrier and reactant gases, the Ta sputtering current, and the length of the gas aggregation region influence the size, composition, and morphology of the NPs. AFM images revealed the preferential

alignment of all three types of NPs along the step edges of HOPG, resulting in the formation of extended parallel linear chains. TEM images revealed that the Ta-butanol and Ta-heptane NPs have higher contrast crystalline cores surrounded by lower contrast regions composed of amorphous material. In comparison, TEM images of the Ta-xylene NPs showed them to be of higher contrast throughout compared with the Ta-butanol and Ta-heptane species. Reactive sputtering combined with gas aggregation and SL therefore offers a versatile approach for the preparation of non-noble-metal NPs for catalytic applications. As evidenced by these examples, SL of mass-selected ionic clusters and NPs is uniquely capable of preparing well-defined model systems that may be characterized experimentally and modeled theoretically to determine structure–function relationships of individual clusters and emergent properties of cluster assemblies. These unique capabilities will aid the design of new materials with improved activity, selectivity, and durability for a range of catalytic processes.

3.2. Catalytic Activity of Ligated Clusters. SL of ligated clusters has only recently attracted attention as a means of transferring small cluster ions synthesized in solution onto solid supports for characterization of their structure and reactivity.¹⁸⁰ Reduction synthesis in solution in the presence of organic capping ligands provides access to a broad range of ligated metal and metal alloy clusters for applications in catalysis,^{181–183} optics,¹⁸⁴ molecular electronics,¹⁸⁵ and sensing. The reactivity of such clusters may be tuned by varying the size and composition of the core, ionic charge state, and the number and electronic properties of the ligands. For example, thiolated $\text{Au}_{25}^{+/0/-}$ cluster ions in solution have been shown to exhibit different catalytic activity toward CO_2 reduction, CO oxidation, and O_2 reduction reactions depending on their charge state.¹⁸⁶ Fully ligated clusters synthesized in solution may be completely passivated unless ligands that provide access for reactants to metal active sites on the surface are used during synthesis.¹⁸⁷ Heating or chemical treatments may be used to partially remove ligands from passivated clusters to enable catalytic activity without causing sintering under reaction conditions.^{4,118,119,188}

As previously described, SL combined with CID in the gas phase provides an opportunity to prepare well-characterized model heterogeneous and electrochemical catalysts that are challenging to obtain through conventional reduction synthesis in solution. This approach allowed us to compare the reactivity of the stable $(11,5)^{3+}$ Au-DPPP cluster and its fragment, $(10,4)^{2+}$, soft-landed onto different SAMs.⁷² The reactivity was inferred from the presence of adducts in the TOF-SIMS spectra of the soft-landed cluster ions. Comparison of TOF-SIMS spectra obtained for the $(11,5)^{3+}$ precursor and its fragment, $(10,4)^{2+}$, soft-landed onto FSAMs is shown in Figure 8. In the case of $(11,5)^{3+}$, both $(11,5)^{3+}$ and $(11,5)^{2+}$ are observed in the mass spectrum (Figure 8a), indicating efficient charge retention by this cluster on the FSAM. A smaller abundance of $(10,4)^{2+}$ resulting from fragmentation of $(11,5)^{3+}$ during SIMS analysis is also detected. Of particular importance, no ions are observed at higher m/z for soft-landed $(11,5)^{3+}$. This indicates that fully ligated $(11,5)^{3+}$ is relatively inert and does not interact strongly with the surface or any of the energized species present in the plume of sputtered secondary material during SIMS analysis. In comparison, the TOF-SIMS spectrum of the soft-landed $(10,4)^{2+}$ fragment contains abundant $(11,4)+\text{X}^{2+}$ and $(11,4)+\text{X}^+$ ions (Figure 8b), where $\text{X} = (\text{C}_6\text{H}_5)_2\text{P}(\text{CH}_2)_2$.

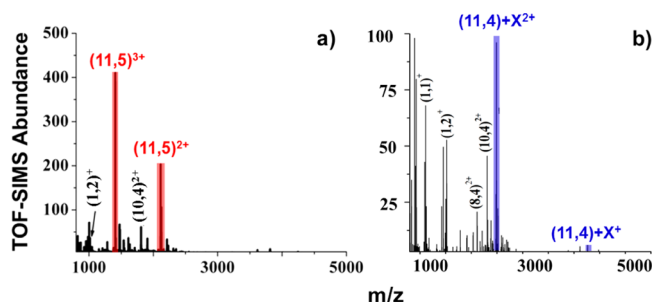


Figure 8. Time-of-flight secondary ion mass spectra of FSAM surfaces following SL of 1×10^{11} (a) $\text{Au}_{11}\text{L}_5^{3+}$ and (b) $\text{Au}_{10}\text{L}_4^{2+}$ ($\text{L} = \text{DPPP}$) ions generated by in-source CID. "X" = $(\text{C}_6\text{H}_5)_3\text{P}(\text{CH}_2)_2\text{P}^n$. Adapted with permission from ref 72. © 2015 Elsevier.

This complex is formed by attachment of a gold atom and a fragment of a DPPP ligand that were generated during SIMS sputtering of the FSAM surface with the energetic primary ion beam (15 keV Ga^+). These results indicate that the $(10,4)^{2+}$ species generated using in-source CID is more reactive than its $(11,5)^{3+}$ precursor ion. Future studies will explore differences in reactivity of such undercoordinated clusters toward gaseous and solution-phase reagents.

3.3. Ion Soft Landing for Fundamental Studies in Energy Storage. Despite considerable progress in the development of energy-storage devices, the design of low-cost systems with high power and energy density remains a major challenge.¹⁸⁹ Fundamental understanding of phenomena occurring at electrode–electrolyte interfaces (EEI) is required to increase the charge–discharge capacity, rate, and life cycle of energy-storage devices.^{189,190} Such studies will benefit from the ability to produce uniform layers of active materials with well-defined composition and coverage. In the past decade, substantial progress has been made in the ability to design carbon electrodes with high non-Faradaic capacitance. A further increase in the electrode performance is achieved by combining the non-Faradaic electrochemical double-layer (EDL) capacitance of high-surface-area carbon electrodes¹⁹¹ with the Faradaic pseudocapacitance of metal oxides.¹⁹² Simultaneous improvements in both the power and energy density have been demonstrated for redox supercapacitors produced using this approach.

Redox-active species are typically deposited onto electrode surfaces using direct painting, ambient air spray, chemical vapor deposition, atomic layer deposition, electrodeposition, and electrospray deposition (ESD).¹⁹³ Although well-suited for macroscale device fabrication, these techniques typically result in deposition of both electrochemically active and inactive components along with solvent molecules and impurities onto electrode surfaces. In contrast, SL enables the preparation of well-defined electrode surfaces by eliminating all undesirable species from the EEI through precise control over the composition, charge state, and kinetic energy of the projectile ion.⁹⁶ As a result, SL provides access to novel materials that cannot be prepared using conventional deposition techniques. Well-defined electrode surfaces prepared using SL are ideally suited for studying the intrinsic activity of electroactive species, characterizing the kinetics of key reactions at the EEI, and understanding the effect of agglomeration and mesoscale phenomena on the stability and efficacy of electrode materials. Fundamental understanding of these phenomena will facilitate

the design of efficient and stable EEI for use in future energy devices.

In the context of redox-supercapacitors, many redox-active inorganic species including RuO_2 ,¹⁹⁴ MnO_2 ,¹⁹⁵ LiFePO_4 ,¹⁹⁶ $\text{Ni}(\text{OH})_2$,¹⁹⁷ and POMs^{198–200} have been considered as pseudocapacitive materials. POMs are stable anionic transition-metal oxide clusters with unique multielectron redox properties^{23,201} that form strong and stable interactions with electrode materials.^{202,203} These properties of POMs make them attractive materials for applications in supercapacitors and batteries.^{201,204} In our studies, we examined the redox activity of POM anions deposited onto SAMs using CV.^{104,105} Redox activity was observed for $\text{PMo}_{12}\text{O}_{40}^{3-}$ (MoPOM) soft-landed onto FSAM and HSAM substrates in the first few CV scans, but this response rapidly disappeared upon continuing cycles, indicating that the POMs were readily washed away from these surfaces. In contrast, strong immobilization of POMs on the NH_3^+ -SAM surface allowed us to examine the effect of the initial charge state of MoPOM (3- vs 2-) on redox properties. The CVs of the MoPOM soft-landed and adsorbed onto the NH_3^+ -SAM surface from solution are shown in Figure 9. The

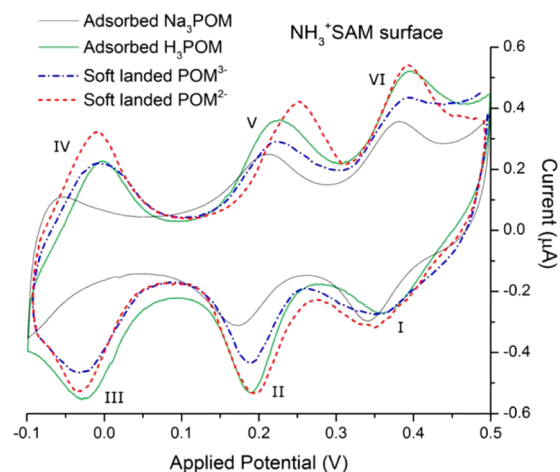


Figure 9. Cyclic voltammograms of POM^{3-} (blue dashed-dotted) and POM^{2-} (red dashed) soft-landed on NH_3^+ -SAM surfaces compared with Na_3POM (gray) and H_3POM (green) adsorbed from solutions. All scans were obtained at a rate of 20 mV s^{-1} after cycling 20 times. All measurements are made with reference to a Ag/AgCl electrode in saturated KCl. Adapted with permission from ref 105.

redox couples observed in acidic aqueous electrolyte are consistent with the two-proton, two-electron processes previously reported for phosphomolybdates in solution.²⁷ It is remarkable that the redox peak currents observed for 2×10^{13} soft-landed MoPOM anions on NH_3^+ -SAM are comparable to those of POM adsorbed from solution. In contrast with MoPOM, no activity was observed for $\text{PW}_{12}\text{O}_{40}^{3-}$ (WPOM) soft-landed onto the NH_3^+ -SAM surface, indicating that WPOM is readily removed from the surface when immersed in 0.5 M H_2SO_4 electrolyte solution.¹⁰⁴ This observation was attributed to the weaker binding of WPOM anions to SAMs.

The pronounced redox activity of soft-landed POM prompted us to examine the utility of SL for the controlled deposition of pseudocapacitive materials onto electrode surfaces. We hypothesized that the activity of POM on carbon electrode surfaces may be enhanced by eliminating electrochemically inactive counter cations from the EEI. To test this hypothesis, we fabricated a first macroscopic high-performance,

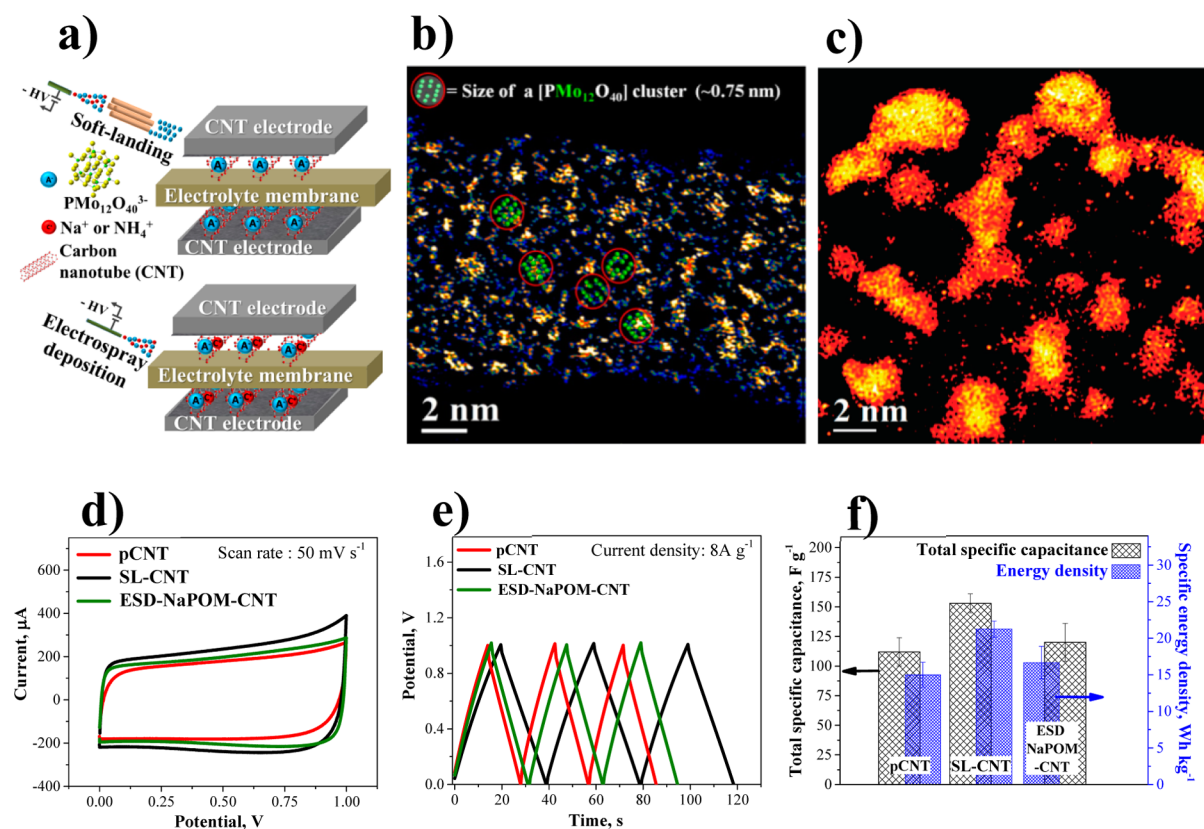


Figure 10. (a) Schematic representation of EEI of redox-supercapacitors fabricated using SL and ambient ESD. Note the absence of counter cations in the device prepared by SL. (b,c) Atomically resolved HAADF-STEM images of SL-CNT and ESD-NaPOM-CNT, respectively; intact SL POM clusters are mapped in panel b (red circles). (d) Representative CV and (e) galvanostatic charge–discharge (GCD) curves of supercapacitors fabricated with pCNT, SL-CNT, and ESD-NaPOM-CNT. (f) Comparison of the total specific capacitance and specific energy density. Approximately 1.5×10^{13} $\text{PMo}_{12}\text{O}_{40}^{3-}$ were deposited in each case. Adapted with permission from ref 96. © 2016 Macmillan Publishers Limited.

nonaqueous redox-supercapacitor device as shown schematically in Figure 10a.⁹⁶ The device is composed of two 1 cm^2 carbon fiber paper electrodes coated with $\sim 25 \mu\text{g}$ of CNTs separated by an ionic liquid membrane. Predetermined amounts of POM are deposited onto CNT electrodes either using SL (SL-CNT) or ambient ESD of pure POM solutions. Surface characterization using HAADF-STEM indicates the presence of discrete $\sim 0.75 \text{ nm}$ diameter $\text{PMo}_{12}\text{O}_{40}^{3-}$ clusters on SL-CNT electrodes (Figure 10b), while substantial agglomeration of POM is observed instead on CNT electrodes fabricated using ESD (Figure 10c).

CVs and galvanostatic charge–discharge (GCD) curves obtained for pristine CNT electrodes (pCNT), SL-CNT, and electrodes prepared using ambient ESD of $\text{Na}_3\text{PMo}_{12}\text{O}_{40}$ (ESD-NaPOM-CNT) are shown in Figure 10d and 10e, respectively. Rectangular-shaped CVs obtained for all fabricated supercapacitors confirm ideal capacitive-like behavior of the devices. Almost symmetrical triangular-shaped GCD curves indicate fast transmission of ions at the EEI. The total specific capacitance and energy density of the SL-CNT, shown in Figure 10f, are ~ 36 and 27% higher than the values obtained for pCNT and ESD-NaPOM-CNT, respectively. The SL electrodes were also found to have 60% higher capacity retention after 1000 GCD cycles compared with those prepared by ESD.⁹⁶ Remarkably, the maximum Faradaic capacitance of the SL electrodes was achieved with only 1.5×10^{13} POM anions ($\sim 50 \text{ ng}$) deposited onto $25 \mu\text{g}$ of CNT, whereas the ESD electrodes required twice this amount of material to achieve comparable performance. Any further addition of POM

led to a decrease in the total specific capacitance indicating the high energy-storage capacity of nanogram quantities of POM anions. These results demonstrate the superior performance of SL-CNT in terms of both specific capacitance and long-term stability.⁹⁶ Detailed characterization of electrode surfaces using XPS, SEM, and STEM indicates that aggregation of redox-active POM and the presence of electrochemically inactive counter cations at the EEI are largely responsible for the lower performance of POM-based supercapacitors fabricated from solution. It follows that higher performance and longer stability of the EEI can be achieved through uniform deposition of discrete redox-active species and elimination of inactive counterions or solvent molecules.⁹⁶

3.4. Electrochemical Characterization of Precisely-Selected Ions. In addition to fabrication of electrodes for energy-storage devices, SL can be used to obtain fundamental understanding of electrochemical processes at the EEI by performing electrochemical characterization of precisely selected ions. Previously, Anderson and coworkers used a specially designed in-vacuum liquid electrochemical cell^{205,206} to perform in situ characterization of SL metal clusters and demonstrated substantial damage of GC electrodes containing SL Pt clusters upon exposure to air and water. These studies highlighted the important role of SL and characterization of the EEI in a well-controlled environment. Our group is actively working on developing a new capability to perform in situ electrochemical characterization of directly deposited mass- and charge-selected ions produced using an ESI source and dissociated clusters produced using in-source CID as well as

bare metal clusters produced using magnetron sputtering, which allows one to gain novel insights into electrode kinetics at well-defined EEI in a controlled environment. In brief, Penner and Gogotsi recently pointed out the current need to explore fundamental aspects of electrochemistry that are relevant to various energy applications.²⁰⁷ SL can be used to gain unprecedented information about the electrochemical processes occurring at EEI via fabrication and characterization of precisely defined systems. This will facilitate rational design of high-performance next-generation electrodes for various energy technologies.

3.5. Molecular Electronics. Quantized charging of ligated metal clusters, resulting from their subattofarad capacitance,^{208,209} as well as charge transport to clusters through SAMs^{70–72} have consequences for the design of nanoelectronic devices and fabrication of functionalized electrodes,²¹⁰ organic thin-film transistors,²¹¹ and organic memory.²¹² It has been demonstrated that the local environment at surfaces exerts a large influence on electron transfer through metal NPs in contact with SAMs.^{213,214} As previously mentioned, alkanethiols exhibit no barrier to charge transfer, while perfluorinated monolayers necessitate potentials of up to 1.5 V to promote electron transfer.¹⁵³ Because of the wide range of properties obtainable with different combinations of supported metal clusters and SAMs, it is clearly desirable to investigate charge-transport phenomena at supported clusters with well-defined geometry and chemical functionality. In addition, it is useful to measure charge transport by a large number of identical clusters distributed over millimeter length scales so that the influence of different surface domains, boundaries, and potential defects in the monolayer are represented.

4. SUMMARY AND FUTURE CHALLENGES

SL is a versatile technique for the highly controlled preparation of well-defined interfaces for studies in catalysis and energy storage. It has been demonstrated that the charge state of the ion may be controlled by varying the coverage of the soft-landed species and carefully tailoring the properties of the surface. Although charge reduction by soft-landed cations is quite efficient, relatively high barriers for electron detachment from anions are responsible for more efficient charge retention by negatively charged species. This is particularly important because the redox activity of soft-landed ions and their binding to surfaces may be affected by their charge state. SL of redox-active POM anions onto CNT electrodes has been shown to produce highly dispersed uniform monolayers of pure pseudocapacitive material, resulting in a substantial increase in both the capacitance and stability of the resulting EEI. Furthermore, SL of alloy and hybrid organic–inorganic clusters and NPs has been demonstrated as a means of preparing surfaces containing electrochemically active non-noble species for studying the effect of composition, size, and coverage on the efficiency of catalytic materials.

Much has been learned about the reactivity of individual sparsely deposited complex ions on well-defined surfaces. In addition, first experiments utilizing technologically relevant substrates and ionic cluster assemblies have been reported. These studies have already demonstrated the unique power of SL for the preparation of electrodes containing pure redox active ionic species and for understanding the effect of assemblies on the overall electrocatalytic activity of supported nanomaterials. For example, it has been shown that as interparticle distance decreases, increasing diffusional overlap

occurs between adjacent species in solution in terms of reactant and intermediate transport.²¹⁵ Furthermore, assemblies of supported clusters may structure the surrounding solvent, resulting in the formation of highly efficient catalytic hot spots at critical edge-to-edge distances.⁶⁹ Future studies will focus on understanding how ion–support and ion–ion or ion–molecule interactions evolve with increasing coverage from the limit of isolated ionic and neutral soft-landed species toward high-coverage assemblies and what effect this has on the macroscopic properties of the resulting material. The support may facilitate or impede agglomeration of deposited species that affects the surface-to-volume ratio of the active material. In addition, charge transfer between supports and complex ions may enhance their catalytic activity and stability.²¹⁶ The collective properties of soft-landed assemblies produced at high coverage, therefore, are affected by interactions within the ensemble of complex molecules along with interactions with support and solvent molecules. Understanding these mesoscale emergent properties will be a fruitful area of inquiry for SL in the future.²¹⁷

■ AUTHOR INFORMATION

Corresponding Authors

*J.L.: E-mail: Julia.Laskin@pnnl.gov. Tel: (509)-371-6136.

*G.E.J.: E-mail: Grant.Johnson@pnnl.gov. Tel: (509)-371-6753.

Notes

The authors declare no competing financial interest.

Biographies



Julia Laskin is currently a Laboratory Fellow at Pacific Northwest National Laboratory (PNNL). She received her M.Sc. in physics from the Leningrad Polytechnical Institute (1990) and her Ph.D. in physical chemistry from the Hebrew University of Jerusalem (1998). Her research is focused on obtaining a fundamental understanding of the interactions of complex ions and molecules with surfaces for improved identification of large molecules using mass spectrometry and for selective modification of substrates using beams of mass-selected ions (ion soft landing). These studies utilize unique mass spectrometry instrumentation specially designed for studying physical and chemical phenomena underlying ion-surface collisions. She also leads the development of nanospray desorption electrospray ionization (nano-DESI) mass spectrometry for imaging of fully hydrated biological samples in their native environment and for chemical analysis of complex mixtures directly from solid substrates. She has published >195 papers including several book chapters review articles and holds 3 patents. Her research has been recognized with several prestigious awards including Presidential Early Career Award (PECASE) in 2007,

ASMS Biemann Medal in 2008, Inaugural Rising Star Award of the ACS Women Chemists Committee, 2011, and others. She is a member of the Editorial Board of *Analyst*, *Journal of the American Society for Mass Spectrometry*, *Russian Mass Spectrometry Journal*, *Advanced Structural and Chemical Imaging*, and *Frontiers in Microbiology*.



Grant E. Johnson obtained his B.S. degree in chemistry from the University of Delaware in 2002, where he studied solvation in supercritical fluids under Robert Wood. He received his Ph.D. in physical chemistry from The Pennsylvania State University under A. W. Castleman Jr. in 2009. He was awarded a National Science Foundation fellowship in 2006 to study computational chemistry with Vlasta Bonacic-Koutecky at the Humboldt University in Berlin, Germany. He received a Department of Energy fellowship to attend the meeting of Nobel Laureates in chemistry in Lindau, Germany. He was awarded the inaugural Linus Pauling Postdoctoral Fellowship at the Pacific Northwest National Laboratory (PNNL) from 2010 to 2012. He is currently a scientist in the Chemical Physics and Analysis program at PNNL working on the development of soft-landing instrumentation for the controlled preparation and characterization of energy-related materials.



Venkateshkumar Prabhakaran received his B.S. in chemical and electrochemical engineering from the Central Electrochemical Research Institute, India in 2009 and his Ph.D. in chemical engineering from the Illinois Institute of Technology under Vijay Ramani in 2014. During his Ph.D, he investigated chemical degradation kinetics and mitigation strategies in polymer electrolyte fuel cells using in situ fluorescence spectroscopy. He is now a postdoctoral research associate at Pacific Northwest National Laboratory. His current research interests focus on the preparation of novel electrode materials using soft and reactive landing of ions, the development of in situ and in-operando techniques to gain fundamental understanding of electrochemical processes at well-defined electrode–electrolyte interfaces

prepared with soft-landed ions, and the application of soft-landing techniques in various electrochemical technologies.

■ ACKNOWLEDGMENTS

Our ongoing research involving soft landing of mass-selected ions on surfaces is supported by the U.S. Department of Energy (DOE), Office of Basic Energy Sciences, Chemical Sciences, Geosciences & Biosciences Division. G.E.J. acknowledges support from the Laboratory Directed Research and Development Program at the Pacific Northwest National Laboratory (PNNL). The research is performed using EMSL, a national scientific user facility sponsored by the DOE's Office of Biological and Environmental Research and located at PNNL. PNNL is operated by Battelle for the DOE under Contract DE-AC05-76RL01830.

■ REFERENCES

- (1) Zhou, Z.-Y.; Tian, N.; Li, J.-T.; Broadwell, I.; Sun, S.-G. Nanomaterials of High Surface Energy with Exceptional Properties in Catalysis and Energy Storage. *Chem. Soc. Rev.* **2011**, *40*, 4167–4185.
- (2) Astruc, D.; Lu, F.; Aranzaes, J. R. Nanoparticles as Recyclable Catalysts: The Frontier between Homogeneous and Heterogeneous Catalysis. *Angew. Chem., Int. Ed.* **2005**, *44*, 7852–7872.
- (3) Vajda, S.; White, M. G. Catalysis Applications of Size-Selected Cluster Deposition. *ACS Catal.* **2015**, *5*, 7152–7176.
- (4) Li, G.; Jin, R. C. Atomically Precise Gold Nanoclusters as New Model Catalysts. *Acc. Chem. Res.* **2013**, *46*, 1749–1758.
- (5) Zhang, Q.; Uchaker, E.; Candelaria, S. L.; Cao, G. Nanomaterials for Energy Conversion and Storage. *Chem. Soc. Rev.* **2013**, *42*, 3127–3171.
- (6) Arico, A. S.; Bruce, P.; Scrosati, B.; Tarascon, J.-M.; van Schalkwijk, W. Nanostructured Materials for Advanced Energy Conversion and Storage Devices. *Nat. Mater.* **2005**, *4*, 366–377.
- (7) Krug, H. F.; Wick, P. Nanotoxicology: An Interdisciplinary Challenge. *Angew. Chem., Int. Ed.* **2011**, *50*, 1260–1278.
- (8) Dreaden, E. C.; Mackey, M. A.; Huang, X. H.; Kang, B.; El-Sayed, M. A. Beating Cancer in Multiple Ways Using Nanogold. *Chem. Soc. Rev.* **2011**, *40*, 3391–3404.
- (9) Schooss, D.; Weis, P.; Hampe, O.; Kappes, M. M. Determining the Size-Dependent Structure of Ligand-Free Gold-Cluster Ions. *Philos. Trans. R. Soc., A* **2010**, *368*, 1211–1243.
- (10) Wang, B.; Yoon, B.; Konig, M.; Fukamori, Y.; Esch, F.; Heiz, U.; Landman, U. Size-Selected Monodisperse Nanoclusters on Supported Graphene: Bonding, Isomerism, and Mobility. *Nano Lett.* **2012**, *12*, 5907–5912.
- (11) Hakkinen, H.; Yoon, B.; Landman, U.; Li, X.; Zhai, H. J.; Wang, L. S. On the Electronic and Atomic Structures of Small Au_n⁻ (N = 4–14) Clusters: A Photoelectron Spectroscopy and Density-Functional Study. *J. Phys. Chem. A* **2003**, *107*, 6168–6175.
- (12) Walter, M.; Akola, J.; Lopez-Acevedo, O.; Jadzinsky, P. D.; Calero, G.; Ackerson, C. J.; Whetten, R. L.; Gronbeck, H.; Hakkinen, H. A Unified View of Ligand-Protected Gold Clusters as Superatom Complexes. *Proc. Natl. Acad. Sci. U. S. A.* **2008**, *105*, 9157–9162.
- (13) Schwarz, H. Doping Effects in Cluster-Mediated Bond Activation. *Angew. Chem., Int. Ed.* **2015**, *54*, 10090.
- (14) Johnson, G. E.; Mitric, R.; Bonacic-Koutecky, V.; Castleman, A. W. Clusters as Model Systems for Investigating Nanoscale Oxidation Catalysis. *Chem. Phys. Lett.* **2009**, *475*, 1–9.
- (15) Claridge, S. A.; Castleman, A. W.; Khanna, S. N.; Murray, C. B.; Sen, A.; Weiss, P. S. Cluster-Assembled Materials. *ACS Nano* **2009**, *3*, 244–255.
- (16) Dietz, T. G.; Duncan, M. A.; Powers, D. E.; Smalley, R. E. Laser Production of Supersonic Metal Cluster Beams. *J. Chem. Phys.* **1981**, *74*, 6511–6512.
- (17) Duncan, M. A. Invited Review Article: Laser Vaporization Cluster Sources. *Rev. Sci. Instrum.* **2012**, *83*, 041101.

- (18) Pratontep, S.; Carroll, S. J.; Xirouchaki, C.; Streun, M.; Palmer, R. E. Size-Selected Cluster Beam Source Based on Radio Frequency Magnetron Plasma Sputtering and Gas Condensation. *Rev. Sci. Instrum.* **2005**, *76*, 045103.
- (19) Palmer, R. E.; Cao, L.; Yin, F. Note: Proof of Principle of a New Type of Cluster Beam Source with Potential for Scale-Up. *Rev. Sci. Instrum.* **2016**, *87*, 046103.
- (20) Qian, H. F.; Zhu, M. Z.; Wu, Z. K.; Jin, R. C. Quantum Sized Gold Nanoclusters with Atomic Precision. *Acc. Chem. Res.* **2012**, *45*, 1470–1479.
- (21) Templeton, A. C.; Wuelfing, W. P.; Murray, R. W. Monolayer-Protected Cluster Molecules. *Acc. Chem. Res.* **2000**, *33*, 27–36.
- (22) Long, D. L.; Burkholder, E.; Cronin, L. Polyoxometalate Clusters, Nanostructures and Materials: From Self Assembly to Designer Materials and Devices. *Chem. Soc. Rev.* **2007**, *36*, 105–121.
- (23) Long, D. L.; Tsunashima, R.; Cronin, L. Polyoxometalates: Building Blocks for Functional Nanoscale Systems. *Angew. Chem., Int. Ed.* **2010**, *49*, 1736–1758.
- (24) Song, Y.-F.; Tsunashima, R. Recent Advances on Polyoxometalate-Based Molecular and Composite Materials. *Chem. Soc. Rev.* **2012**, *41*, 7384–7402.
- (25) Coronado, E.; Gómez-García, C. J. Polyoxometalate-Based Molecular Materials. *Chem. Rev.* **1998**, *98*, 273–296.
- (26) Liu, C. G.; Guan, X. H. Computational Study on Redox-Switchable Second-Order Nonlinear Optical Properties of Totally Inorganic Keggin-Type Polyoxometalate Complexes. *J. Phys. Chem. C* **2013**, *117*, 7776–7783.
- (27) Sadakane, M.; Steckhan, E. Electrochemical Properties of Polyoxometalates as Electrocatalysts. *Chem. Rev.* **1998**, *98*, 219–237.
- (28) Kortz, U.; Müller, A.; van Slageren, J.; Schnack, J.; Dalal, N. S.; Dressel, M. Polyoxometalates: Fascinating Structures, Unique Magnetic Properties. *Coord. Chem. Rev.* **2009**, *253*, 2315–2327.
- (29) Yamase, T. Photo- and Electrochromism of Polyoxometalates and Related Materials. *Chem. Rev.* **1998**, *98*, 307–326.
- (30) Wang, S.-S.; Yang, G.-Y. Recent Advances in Polyoxometalate-Catalyzed Reactions. *Chem. Rev.* **2015**, *115*, 4893–4962.
- (31) Notestein, J. M.; Katz, A. Enhancing Heterogeneous Catalysis Through Cooperative Hybrid Organic–Inorganic Interfaces. *Chem. - Eur. J.* **2006**, *12*, 3954–3965.
- (32) Coperet, C.; Chabanas, M.; Saint-Arroman, R. P.; Basset, J. M. Homogeneous and Heterogeneous Catalysis: Bridging the Gap through Surface Organometallic Chemistry. *Angew. Chem., Int. Ed.* **2003**, *42*, 156–181.
- (33) Zeitler, K. Photoredox Catalysis with Visible Light. *Angew. Chem., Int. Ed.* **2009**, *48*, 9785–9789.
- (34) Wong, W.-Y.; Ho, C.-L. Organometallic Photovoltaics: A New and Versatile Approach for Harvesting Solar Energy Using Conjugated Polymetalloynes. *Acc. Chem. Res.* **2010**, *43*, 1246–1256.
- (35) Heiz, U.; Vanolli, F.; Trento, L.; Schneider, W. D. Chemical Reactivity of Size-Selected Supported Clusters: An Experimental Setup. *Rev. Sci. Instrum.* **1997**, *68*, 1986–1994.
- (36) Yin, C.; Tyo, E.; Kuchta, K.; von Issendorff, B.; Vajda, S. Atomically Precise (Catalytic) Particles Synthesized by a Novel Cluster Deposition Instrument. *J. Chem. Phys.* **2014**, *140*, 174201.
- (37) Popok, V. N.; Barke, I.; Campbell, E. E. B.; Meiwes-Broer, K. H. Cluster-Surface Interaction: From Soft Landing to Implantation. *Surf. Sci. Rep.* **2011**, *66*, 347–377.
- (38) Armentrout, P. B. Reactions and Thermochemistry of Small Transition Metal Cluster Ions. *Annu. Rev. Phys. Chem.* **2001**, *52*, 423–461.
- (39) Ho, J.; Ervin, K. M.; Lineberger, W. C. Photoelectron-Spectroscopy of Metal Cluster Anions - Cu_n^- , Ag_n^- , and Au_n^- . *J. Chem. Phys.* **1990**, *93*, 6987–7002.
- (40) Furche, F.; Ahlrichs, R.; Weis, P.; Jacob, C.; Gilb, S.; Bierweiler, T.; Kappes, M. M. The Structures of Small Gold Cluster Anions as Determined by a Combination of Ion Mobility Measurements and Density Functional Calculations. *J. Chem. Phys.* **2002**, *117*, 6982.
- (41) Asmis, K. R.; Sauer, J. Mass-Selective Vibrational Spectroscopy of Vanadium Oxide Cluster Ions. *Mass Spectrom. Rev.* **2007**, *26*, 542–562.
- (42) Johnson, G. E.; Tyo, E. C.; Castleman, A. W. Cluster Reactivity Experiments: Employing Mass Spectrometry to Investigate the Molecular Level Details of Catalytic Oxidation Reactions. *Proc. Natl. Acad. Sci. U. S. A.* **2008**, *105*, 18108–18113.
- (43) Fernando, A.; Weerawardene, K. L. D. M.; Karimova, N. V.; Aikens, C. M. Quantum Mechanical Studies of Large Metal, Metal Oxide, and Metal Chalcogenide Nanoparticles and Clusters. *Chem. Rev.* **2015**, *115*, 6112–6216.
- (44) Li, Z. H.; Truhlar, D. G. Nanothermodynamics of Metal Nanoparticles. *Chem. Sci.* **2014**, *5*, 2605–2624.
- (45) Lang, S. M.; Bernhardt, T. M. Gas Phase Metal Cluster Model Systems for Heterogeneous Catalysis. *Phys. Chem. Chem. Phys.* **2012**, *14*, 9255–9269.
- (46) Cramer, C. J.; Truhlar, D. G. Density Functional Theory for Transition Metals and Transition Metal Chemistry. *Phys. Chem. Chem. Phys.* **2009**, *11*, 10757–10816.
- (47) Goldby, I. M.; vonIssendorff, B.; Kuipers, L.; Palmer, R. E. Gas Condensation Source for Production and Deposition of Size-Selected Metal Clusters. *Rev. Sci. Instrum.* **1997**, *68*, 3327–3334.
- (48) Fields-Zinna, C. A.; Sardar, R.; Beasley, C. A.; Murray, R. W. Electrospray Ionization Mass Spectrometry of Intrinsically Cationized Nanoparticles, $[\text{Au}_{144/146}(\text{Sc}_{11}\text{H}_{22}\text{N}(\text{CH}_2\text{CH}_3)^3)_X(\text{S}(\text{CH}_2)_8\text{CH}_3)_Y]^{X+}$. *J. Am. Chem. Soc.* **2009**, *131*, 16266–16271.
- (49) Li, A. Y.; Luo, Q. J.; Park, S. J.; Cooks, R. G. Synthesis and Catalytic Reactions of Nanoparticles Formed by Electrospray Ionization of Coinage Metals. *Angew. Chem., Int. Ed.* **2014**, *53*, 3147–3150.
- (50) Qian, H. F.; Zhu, Y.; Jin, R. C. Size-Focusing Synthesis, Optical and Electrochemical Properties of Monodisperse $\text{Au}_{38}(\text{Sc}_2\text{H}_4\text{ph})_{24}$ Nanoclusters. *ACS Nano* **2009**, *3*, 3795–3803.
- (51) Cyriac, J.; Pradeep, T.; Kang, H.; Souda, R.; Cooks, R. G. Low-Energy Ionic Collisions at Molecular Solids. *Chem. Rev.* **2012**, *112*, 5356–5411.
- (52) Verbeck, G.; Hoffmann, W.; Walton, B. Soft-Landing Preparative Mass Spectrometry. *Analyst* **2012**, *137*, 4393–4407.
- (53) Johnson, G. E.; Hu, Q. C.; Laskin, J. Soft Landing of Complex Molecules on Surfaces. *Annu. Rev. Anal. Chem.* **2011**, *4*, 83–104.
- (54) Johnson, G. E.; Gunaratne, D.; Laskin, J. Soft- and Reactive Landing of Ions Onto Surfaces: Concepts and Applications. *Mass Spectrom. Rev.* **2016**, *35*, 439–79.
- (55) Grill, V.; Shen, J.; Evans, C.; Cooks, R. G. Collisions of Ions with Surfaces at Chemically Relevant Energies: Instrumentation and Phenomena. *Rev. Sci. Instrum.* **2001**, *72*, 3149–3179.
- (56) Gologan, B.; Wiseman, J. M.; Cooks, R. G. Ion Soft Landing: Instrumentation, Phenomena, and Applications. In *Principles of Mass Spectrometry Applied to Biomolecules*; Laskin, J., Lifshitz, C., Eds.; John Wiley & Sons, Inc.: Hoboken, NJ, 2006.
- (57) Tang, J.; Verrelli, E.; Tsoukalas, D. Assembly of Charged Nanoparticles Using Self-Electrodynamic Focusing. *Nanotechnology* **2009**, *20*, 365605.
- (58) Laskin, J.; Wang, P.; Hadjar, O. Soft-Landing of Peptide Ions Onto Self-Assembled Monolayer Surfaces: An Overview. *Phys. Chem. Chem. Phys.* **2008**, *10*, 1079–1090.
- (59) Alvarez, J.; Futrell, J. H.; Laskin, J. Soft-Landing of Peptides Onto Self-Assembled Monolayer Surfaces. *J. Phys. Chem. A* **2006**, *110*, 1678–1687.
- (60) Volny, M.; Elam, W. T.; Branca, A.; Ratner, B. D.; Turecek, F. Preparative Soft and Reactive Landing of Multiply Charged Protein Ions on a Plasma-Treated Metal Surface. *Anal. Chem.* **2005**, *77*, 4890–4896.
- (61) Ouyang, Z.; Takats, Z.; Blake, T. A.; Gologan, B.; Guymon, A. J.; Wiseman, J. M.; Oliver, J. C.; Davisson, V. J.; Cooks, R. G. Preparing Protein Microarrays by Soft-Landing of Mass-Selected Ions. *Science* **2003**, *301*, 1351–1354.
- (62) Deng, Z. T.; Thontasen, N.; Malinowski, N.; Rinke, G.; Harnau, L.; Rauschenbach, S.; Kern, K. A Close Look at Proteins:

Submolecular Resolution of Two- and Three-Dimensionally Folded Cytochrome C at Surfaces. *Nano Lett.* **2012**, *12*, 2452–2458.

(63) Johnson, G. E.; Laskin, J. Preparation of Surface Organometallic Catalysts by Gas-Phase Ligand Stripping and Reactive Landing of Mass-Selected Ions. *Chem. - Eur. J.* **2010**, *16*, 14433–14438.

(64) Peng, W. P.; Johnson, G. E.; Fortmeyer, I. C.; Wang, P.; Hadjar, O.; Cooks, R. G.; Laskin, J. Redox Chemistry in Thin Layers of Organometallic Complexes Prepared Using Ion Soft Landing. *Phys. Chem. Chem. Phys.* **2011**, *13*, 267–75.

(65) Nagaoka, S.; Ikemoto, K.; Horiuchi, K.; Nakajima, A. Soft- and Reactive-Landing of Cr(Aniline)₂ Sandwich Complexes onto Self-Assembled Monolayers: Separation Between Functional and Binding Sites. *J. Am. Chem. Soc.* **2011**, *133*, 18719–18727.

(66) Pepi, F.; Tata, A.; Garzoli, S.; Giacomello, P.; Ragno, R.; Patsilina, A.; Di Fusco, M.; D'Annibale, A.; Cannistraro, S.; Baldacchini, C.; et al. Chemically Modified Multiwalled Carbon Nanotubes Electrodes with Ferrocene Derivatives Through Reactive Landing. *J. Phys. Chem. C* **2011**, *115*, 4863–4871.

(67) Hu, Q. C.; Laskin, J. Reactive Landing of Dendrimer Ions Onto Activated Self-Assembled Monolayer Surfaces. *J. Phys. Chem. C* **2014**, *118*, 2602–2608.

(68) Tyo, E. C.; Vajda, S. Catalysis by Clusters with Precise Numbers of Atoms. *Nat. Nanotechnol.* **2015**, *10*, 577–588.

(69) Nesselberger, M.; Roefzaad, M.; Hamou, R. F.; Biedermann, P. U.; Schweinberger, F. F.; Kunz, S.; Schloegl, K.; Wiberg, G. K. H.; Ashton, S.; Heiz, U.; et al. The Effect of Particle Proximity on the Oxygen Reduction Rate of Size-Selected Platinum Clusters. *Nat. Mater.* **2013**, *12*, 919–924.

(70) Johnson, G. E.; Priest, T.; Laskin, J. Charge Retention by Gold Clusters on Surfaces Prepared Using Soft Landing of Mass Selected Ions. *ACS Nano* **2012**, *6*, 573–582.

(71) Johnson, G. E.; Priest, T.; Laskin, J. Coverage-Dependent Charge Reduction of Cationic Gold Clusters on Surfaces Prepared Using Soft Landing of Mass-Selected Ions. *J. Phys. Chem. C* **2012**, *116*, 24977–24986.

(72) Johnson, G. E.; Laskin, J. Soft Landing of Mass-Selected Gold Clusters: Influence of Ion and Ligand on Charge Retention and Reactivity. *Int. J. Mass Spectrom.* **2015**, *377*, 205–213.

(73) Yoon, B.; Hakkinen, H.; Landman, U.; Worz, A. S.; Antonietti, J. M.; Abbet, S.; Judai, K.; Heiz, U. Charging Effects on Bonding and Catalyzed Oxidation of CO on Au₈ Clusters on MgO. *Science* **2005**, *307*, 403–407.

(74) Plant, S. R.; Cao, L.; Palmer, R. E. Atomic Structure Control of Size-Selected Gold Nanoclusters During Formation. *J. Am. Chem. Soc.* **2014**, *136*, 7559–62.

(75) Habibpour, V.; Song, M. Y.; Wang, Z. W.; Cookson, J.; Brown, C. M.; Bishop, P. T.; Palmer, R. E. Novel Powder-Supported Size-Selected Clusters for Heterogeneous Catalysis Under Realistic Reaction Conditions. *J. Phys. Chem. C* **2012**, *116*, 26295–26299.

(76) Miller, S. A.; Luo, H.; Pachuta, S. J.; Cooks, R. G. Soft-Landing of Polyatomic Ions at Fluorinated Self-Assembled Monolayer Surfaces. *Science* **1997**, *275*, 1447–1450.

(77) Laskin, J.; Wang, P.; Hadjar, O. Soft-Landing of Co^{III}(Salen)⁺ and Mn^{III}(Salen)⁺ on Self-Assembled Monolayer Surfaces. *J. Phys. Chem. C* **2010**, *114*, 5305–5311.

(78) Mitsui, M.; Nagaoka, S.; Matsumoto, T.; Nakajima, A. Soft-Landing Isolation of Vanadium-Benzene Sandwich Clusters on a Room-Temperature Substrate Using N-Alkanethiolate Self-Assembled Monolayer Matrixes. *J. Phys. Chem. B* **2006**, *110*, 2968–2971.

(79) Morris, M. R.; Riederer, D. E.; Winger, B. E.; Cooks, R. G.; Ast, T.; Chidsey, C. E. D. Ion Surface Collisions at Functionalized Self-Assembled Monolayer Surfaces. *Int. J. Mass Spectrom. Ion Processes* **1992**, *122*, 181–217.

(80) Cooks, R. G.; Ast, T.; Pradeep, T.; Wysocki, V. Reactions of Ions with Organic-Surfaces. *Acc. Chem. Res.* **1994**, *27*, 316–323.

(81) Bajales, N.; Schmaus, S.; Miyamashi, T.; Wulfhekel, W.; Wilhelm, J.; Walz, M.; Stendel, M.; Bagrets, A.; Evers, F.; Ulas, S. C₅₈ on Au(111): A Scanning Tunneling Microscopy Study. *J. Chem. Phys.* **2013**, *138*, 104703.

(82) Hauptmann, N.; Scheil, K.; Gopakumar, T. G.; Otte, F. L.; Schütt, C.; Herges, R.; Berndt, R. Surface Control of Alkyl Chain Conformations and 2d Chiral Amplification. *J. Am. Chem. Soc.* **2013**, *135*, 8814–8817.

(83) Hamann, C.; Woltmann, R.; Hong, I. P.; Hauptmann, N.; Karan, S.; Berndt, R. Ultrahigh Vacuum Deposition of Organic Molecules by Electrospray Ionization. *Rev. Sci. Instrum.* **2011**, *82*, 033903.

(84) Mayer, P. S.; Tureček, F.; Lee, H.-N.; Scheidemann, A. A.; Olney, T. N.; Schumacher, F.; Štrop, P.; Smrčina, M.; Pátek, M.; Schirlin, D. Preparative Separation of Mixtures by Mass Spectrometry. *Anal. Chem.* **2005**, *77*, 4378–4384.

(85) Landman, U.; Yoon, B.; Zhang, C.; Heiz, U.; Arenz, M. Factors in Gold Nanocatalysis: Oxidation of Co in the Non-Scalable Size Regime. *Top. Catal.* **2007**, *44*, 145–158.

(86) Kaden, W. E.; Wu, T. P.; Kunkel, W. A.; Anderson, S. L. Electronic Structure Controls Reactivity of Size-Selected Pd Clusters Adsorbed on TiO₂ Surfaces. *Science* **2009**, *326*, 826–829.

(87) Tong, X.; Benz, L.; Kemper, P.; Metiu, H.; Bowers, M. T.; Buratto, S. K. Intact Size-Selected Aun Clusters on a TiO₂(110)-(1 × 1) Surface at Room Temperature. *J. Am. Chem. Soc.* **2005**, *127*, 13516–13518.

(88) Zhu, J.; Giordano, L.; Lin, S. J.; Fang, Z. X.; Li, Y.; Huang, X.; Zhang, Y. F.; Pacchioni, G. Tuning the Charge State of (W₆O₃)₃ Nanoclusters Deposited on MgO/Ag(001) Films. *J. Phys. Chem. C* **2012**, *116*, 17668–17675.

(89) Mazzei, F.; Favero, G.; Frascioni, M.; Tata, A.; Pepi, F. Electron-Transfer Kinetics of Microperoxidase-11 Covalently Immobilised onto the Surface of Multi-Walled Carbon Nanotubes by Reactive Landing of Mass-Selected Ions. *Chem. - Eur. J.* **2009**, *15*, 7359–7367.

(90) Wepasnick, K. A.; Li, X.; Mangler, T.; Noessner, S.; Wolke, C.; Grossmann, M.; Gantefoer, G.; Fairbrother, D. H.; Bowen, K. H. Surface Morphologies of Size-Selected Mo_{100+2.5} and (MoO₃)_{67+1.5} Clusters Soft-Landed onto Hopg. *J. Phys. Chem. C* **2011**, *115*, 12299–12307.

(91) Rauschenbach, S.; Stadler, F. L.; Lunedei, E.; Malinowski, N.; Koltsov, S.; Costantini, G.; Kern, K. Electrospray Ion Beam Deposition of Clusters and Biomolecules. *Small* **2006**, *2*, 540–547.

(92) Bottcher, A.; Weis, P.; Bihlmeier, A.; Kappes, M. M. C-58 on Hopg: Soft-Landing Adsorption and Thermal Desorption. *Phys. Chem. Chem. Phys.* **2004**, *6*, 5213–5217.

(93) Dubey, G.; Urcuyo, R.; Abb, S.; Rinke, G.; Burghard, M.; Rauschenbach, S.; Kern, K. Chemical Modification of Graphene Via Hyperthermal Molecular Reaction. *J. Am. Chem. Soc.* **2014**, *136*, 13482–13485.

(94) Gunaratne, K. D. D.; Prabhakaran, V.; Ibrahim, Y. M.; Norheim, R. V.; Johnson, G. E.; Laskin, J. Design and Performance of a High-Flux Electrospray Ionization Source for Ion Soft Landing. *Analyst* **2015**, *140*, 2957–2963.

(95) Badu-Tawiah, A. K.; Wu, C. P.; Cooks, R. G. Ambient Ion Soft Landing. *Anal. Chem.* **2011**, *83*, 2648–2654.

(96) Prabhakaran, V.; Mehdi, B. L.; Ditto, J. J.; Engelhard, M. H.; Wang, B.; Gunaratne, K. D. D.; Johnson, D. C.; Browning, N. D.; Johnson, G. E.; Laskin, J. Rational Design of Efficient Electrode-Electrolyte Interfaces for Solid-State Energy Storage Using Ion Soft Landing. *Nat. Commun.* **2016**, *7*, 11399.

(97) Lu, J.; Cheng, L.; Lau, K. C.; Tyo, E.; Luo, X.; Wen, J.; Miller, D.; Assary, R. S.; Wang, H. H.; Redfern, P.; et al. Effect of the Size-Selective Silver Clusters on Lithium Peroxide Morphology in Lithium-Oxygen Batteries. *Nat. Commun.* **2014**, *5*, 4895.

(98) Cuenya, B. R. Synthesis and Catalytic Properties of Metal Nanoparticles: Size, Shape, Support, Composition, and Oxidation State Effects. *Thin Solid Films* **2010**, *518*, 3127–3150.

(99) Yang, Y. X.; Zhou, J.; Nakayama, M.; Nie, L. Z.; Liu, P.; White, M. G. Surface Dipoles and Electron Transfer at the Metal Oxide-Metal Interface: A 2ppe Study of Size-Selected Metal Oxide Clusters Supported on Cu(111). *J. Phys. Chem. C* **2014**, *118*, 13697–13706.

(100) Zhou, J.; Zhou, J.; Camillone, N.; White, M. G. Electronic Charging of Non-Metallic Clusters: Size-Selected Moxsy Clusters

Supported on an Ultrathin Alumina Film on NiAl(110). *Phys. Chem. Chem. Phys.* **2012**, *14*, 8105–8110.

(101) Molina, L. M.; Hammer, B. Active Role of Oxide Support During Co Oxidation at Au/MgO. *Phys. Rev. Lett.* **2003**, *90*, 206102.

(102) Hadjar, O.; Futrell, J. H.; Laskin, J. First Observation of Charge Reduction and Desorption Kinetics of Multiply Protonated Peptides Soft Landed onto Self-Assembled Monolayer Surfaces. *J. Phys. Chem. C* **2007**, *111*, 18220–18225.

(103) Laskin, J.; Wang, P. Charge Retention by Organometallic Dications on Self-Assembled Monolayer Surfaces. *Int. J. Mass Spectrom.* **2014**, *365*, 187–193.

(104) Gunaratne, K. D. D.; Prabhakaran, V.; Andersen, A.; Johnson, G. E.; Laskin, J. Charge Retention of Soft-Landed Phosphotungstate Keggin Anions on Self-Assembled Monolayers. *Phys. Chem. Chem. Phys.* **2016**, *18*, 9021–9028.

(105) Gunaratne, K. D. D.; Johnson, G. E.; Andersen, A.; Du, D.; Zhang, W. Y.; Prabhakaran, V.; Lin, Y. H.; Laskin, J. Controlling the Charge State and Redox Properties of Supported Polyoxometalates Via Soft Landing of Mass-Selected Ions. *J. Phys. Chem. C* **2014**, *118*, 27611–27622.

(106) Martinez, L.; Diaz, M.; Roman, E.; Ruano, M.; Llamasa, P. D.; Huttel, Y. Generation of Nanoparticles with Adjustable Size and Controlled Stoichiometry: Recent Advances. *Langmuir* **2012**, *28*, 11241–11249.

(107) Zhao, J.; Baibuz, E.; Vernieres, J.; Grammatikopoulos, P.; Jansson, V.; Nagel, M.; Steinhauer, S.; Sowwan, M.; Kuronen, A.; Nordlund, K.; et al. Formation Mechanism of Fe Nanocubes by Magnetron Sputtering Inert Gas Condensation. *ACS Nano* **2016**, *10*, 4684.

(108) Johnson, G. E.; Colby, R.; Laskin, J. Soft Landing of Bare Nanoparticles with Controlled Size, Composition, and Morphology. *Nanoscale* **2015**, *7*, 3491–3503.

(109) Nakayama, M.; Xue, M.; An, W.; Liu, P.; White, M. G. Influence of Cluster-Support Interactions on Reactivity of Size-Selected Nb_xO_y Clusters. *J. Phys. Chem. C* **2015**, *119*, 14756–14768.

(110) Lightstone, J. M.; Patterson, M. J.; Liu, P.; Lofaro, J. C., Jr.; White, M. G. Characterization and Reactivity of the Mo₄₈₆⁺ Cluster Deposited on Au(111). *J. Phys. Chem. C* **2008**, *112*, 11495–11506.

(111) Hu, Q. C.; Wang, P.; Gassman, P. L.; Laskin, J. In Situ Studies of Soft- and Reactive Landing of Mass-Selected Ions Using Infrared Reflection Absorption Spectroscopy. *Anal. Chem.* **2009**, *81*, 7302–7308.

(112) Johnson, G. E.; Lysonski, M.; Laskin, J. In Situ Reactivity and ToF-Sims Analysis of Surfaces Prepared by Soft and Reactive Landing of Mass-Selected Ions. *Anal. Chem.* **2010**, *82*, 5718–5727.

(113) Hadjar, O.; Johnson, G.; Laskin, J.; Kibelka, G.; Shill, S.; Kuhn, K.; Cameron, C.; Kassin, S. Ionccid for Direct Position-Sensitive Charged-Particle Detection: From Electrons and Kev Ions to Hyperthermal Biomolecular Ions. *J. Am. Soc. Mass Spectrom.* **2011**, *22*, 612–23.

(114) Johnson, G. E.; Hadjar, O.; Laskin, J. Characterization of the Ion Beam Focusing in a Mass Spectrometer Using an Ionccid Detector. *J. Am. Soc. Mass Spectrom.* **2011**, *22*, 1388–94.

(115) McLuckey, S. A.; Goeringer, D. E. Slow Heating Methods in Tandem Mass Spectrometry. *J. Mass Spectrom.* **1997**, *32*, 461–474.

(116) Gronert, S. Mass Spectrometric Studies of Organic Ion/Molecule Reactions. *Chem. Rev.* **2001**, *101*, 329–360.

(117) Pitteri, S. J.; McLuckey, S. A. Recent Developments in the Ion/Ion Chemistry of High-Mass Multiply Charged Ions. *Mass Spectrom. Rev.* **2005**, *24*, 931–958.

(118) Anderson, D. P.; Alvino, J. F.; Gentleman, A.; Al Qahtani, H.; Thomsen, L.; Polson, M. I. J.; Metha, G. F.; Golovko, V. B.; Andersson, G. G. Chemically-Synthesised, Atomically-Precise Gold Clusters Deposited and Activated on Titania. *Phys. Chem. Chem. Phys.* **2013**, *15*, 3917–3929.

(119) Anderson, D. P.; Adnan, R. H.; Alvino, J. F.; Shipper, O.; Donoeva, B.; Ruzicka, J. Y.; Al Qahtani, H.; Harris, H. H.; Cowie, B.; Aitken, J. B.; et al. Chemically Synthesised Atomically Precise Gold

Clusters Deposited and Activated on Titania. Part II. *Phys. Chem. Chem. Phys.* **2013**, *15*, 14806–14813.

(120) Martin, T. P. Compound Clusters Produced by the Reaction of Elemental Vapors. *J. Chem. Phys.* **1984**, *81*, 4426–4432.

(121) Baker, S. H.; Thornton, S. C.; Edmonds, K. W.; Maher, M. J.; Norris, C.; Binns, C. The Construction of a Gas Aggregation Source for the Preparation of Size-Selected Nanoscale Transition Metal Clusters. *Rev. Sci. Instrum.* **2000**, *71*, 3178–3183.

(122) Haberland, H.; Karrais, M.; Mall, M. A New Type of Cluster and Cluster Ion-Source. *Z. Phys. D: At., Mol. Clusters* **1991**, *20*, 413–415.

(123) Schaffner, M. H.; Jeanneret, J. F.; Patthey, F.; Schneider, W. D. An Ultrahigh Vacuum Sputter Source for in Situ Deposition of Size-Selected Clusters: Ag on Graphite. *J. Phys. D: Appl. Phys.* **1998**, *31*, 3177–3184.

(124) Siekmann, H. R.; Luder, C.; Faehrmann, J.; Lutz, H. O.; Meiwesbroer, K. H. The Pulsed-Arc Cluster Ion-Source (Pacis). *Z. Phys. D: At., Mol. Clusters* **1991**, *20*, 417–420.

(125) Ellis, P. R.; Brown, C. M.; Bishop, P. T.; Yin, J.; Cooke, K.; Terry, W. D.; Liu, J.; Yin, F.; Palmer, R. E. The Cluster Beam Route to Model Catalysts and Beyond. *Faraday Discuss.* **2016**, *188*, 39.

(126) Luo, Y.; Seo, H. O.; Beck, M.; Proch, S.; Kim, Y. D.; Gantefor, G. Parallel Deposition of Size-Selected Clusters: A Novel Technique for Studying Size-Selectivity on the Atomic Scale. *Phys. Chem. Chem. Phys.* **2014**, *16*, 9233–7.

(127) Yen, C. C.; Wang, D. Y.; Chang, L. S.; Shih, M. H.; Shih, H. C. Improving Conversion Efficiency of Dye-Sensitized Solar Cells by Metal Plasma Ion Implantation of Ruthenium Ions. *Thin Solid Films* **2011**, *519*, 4717–4720.

(128) Yuan, L.; Yu, M.; Li, W.; Ji, H. H.; Ren, L. M.; Zhan, K.; Huang, R.; Zhang, X.; Wang, Y. Y.; Zhang, J. Y.; et al. Molecular Dynamic Simulation on Boron Cluster Implantation for Shallow Junction Formation. *Nucl. Instrum. Methods Phys. Res., Sect. B* **2006**, *251*, 390–394.

(129) Ayesh, A. I.; Qamhieh, N.; Mahmoud, S. T.; Alawadhi, H. Fabrication of Size-Selected Bimetallic Nanoclusters Using Magnetron Sputtering. *J. Mater. Res.* **2012**, *27*, 2441–2446.

(130) Shyjumon, I.; Gopinadhan, M.; Helm, C. A.; Smirnov, B. M.; Hippler, R. Deposition of Titanium/Titanium Oxide Clusters Produced by Magnetron Sputtering. *Thin Solid Films* **2006**, *500*, 41–51.

(131) Majeski, M. W.; Bolotin, I. L.; Hanley, L. Cluster Beam Deposition of Cu_{2-x}S Nanoparticles Into Organic Thin Films. *ACS Appl. Mater. Interfaces* **2014**, *6*, 12901–12908.

(132) Balasubramanian, B.; Das, B.; Skomski, R.; Zhang, W. Y.; Sellmyer, D. J. Novel Nanostructured Rare-Earth-Free Magnetic Materials with High Energy Products. *Adv. Mater.* **2013**, *25*, 6090–6093.

(133) Acseente, T.; Negrea, R. F.; Nistor, L. C.; Logofatu, C.; Matei, E.; Birjega, R.; Grisolia, C.; Dinescu, G. Synthesis of Flower-Like Tungsten Nanoparticles by Magnetron Sputtering Combined with Gas Aggregation. *Eur. Phys. J. D* **2015**, *69*, 161.

(134) Polonsky, O.; Kylian, O.; Drabik, M.; Kousal, J.; Solar, P.; Artemenko, A.; Cechvala, J.; Choukourov, A.; Slavinska, D.; Biederman, H. Deposition of Al Nanoparticles and Their Nanocomposites Using a Gas Aggregation Cluster Source. *J. Mater. Sci.* **2014**, *49*, 3352–3360.

(135) Gracia-Pinilla, M. A.; Martinez, E.; Vidaurri, G. S.; Perez-Tijerina, E. Deposition of Size-Selected Cu Nanoparticles by Inert Gas Condensation. *Nanoscale Res. Lett.* **2010**, *5*, 180–188.

(136) Ayesh, A. I.; Qamhieh, N.; Ghamlouche, H.; Thaker, S.; El-Shaer, M. Fabrication of Size-Selected Pd Nanoclusters Using a Magnetron Plasma Sputtering Source. *J. Appl. Phys.* **2010**, *107*, 034317.

(137) Majumdar, A.; Kopp, D.; Ganeva, M.; Datta, D.; Bhattacharyya, S.; Hippler, R. Development of Metal Nanocluster Ion Source Based on Dc Magnetron Plasma Sputtering at Room Temperature. *Rev. Sci. Instrum.* **2009**, *80*, 095103.

- (138) Baker, S. H.; Thornton, S. C.; Keen, A. M.; Preston, T. I.; Norris, C.; Edmonds, K. W.; Binns, C. The Construction of a Gas Aggregation Source for the Preparation of Mass-Selected Ultrasmall Metal Particles. *Rev. Sci. Instrum.* **1997**, *68*, 1853–1857.
- (139) Guo, S. J.; Zhang, S.; Sun, S. H. Tuning Nanoparticle Catalysis for the Oxygen Reduction Reaction. *Angew. Chem., Int. Ed.* **2013**, *52*, 8526–8544.
- (140) Krishnan, G.; Verheijen, M. A.; ten Brink, G. H.; Palasantzas, G.; Kooi, B. J. Tuning Structural Motifs and Alloying of Bulk Immiscible Mo-Cu Bimetallic Nanoparticles by Gas-Phase Synthesis. *Nanoscale* **2013**, *5*, 5375–5383.
- (141) Ferrando, R.; Jellinek, J.; Johnston, R. L. Nanoalloys: From Theory to Applications of Alloy Clusters and Nanoparticles. *Chem. Rev.* **2008**, *108*, 845–910.
- (142) Johnson, G. E.; Colby, R.; Engelhard, M.; Moon, D.; Laskin, J. Soft Landing of Bare Pt Nanoparticles for Electrochemical Reduction of Oxygen. *Nanoscale* **2015**, *7*, 12379–12391.
- (143) Yasumatsu, H.; Hayakawa, T.; Koizumi, S.; Kondow, T. Unisized Two-Dimensional Platinum Clusters on Silicon(111)-7 × 7 Surface Observed with Scanning Tunneling Microscope. *J. Chem. Phys.* **2005**, *123*, 124709.
- (144) Couillard, M.; Pratontep, S.; Palmer, R. E. Metastable Ordered Arrays of Size-Selected Ag Clusters on Graphite. *Appl. Phys. Lett.* **2003**, *82*, 2595–2597.
- (145) Wang, P.; Hadjar, O.; Gassman, P. L.; Laskin, J. Reactive Landing of Peptide Ions on Self-Assembled Monolayer Surfaces: An Alternative Approach for Covalent Immobilization of Peptides on Surfaces. *Phys. Chem. Chem. Phys.* **2008**, *10*, 1512–1522.
- (146) Carroll, S. J.; Seeger, K.; Palmer, R. E. Trapping of Size-Selected Ag Clusters at Surface Steps. *Appl. Phys. Lett.* **1998**, *72*, 305–307.
- (147) Prevel, B.; Bardotti, L.; Fanget, S.; Hannour, A.; Melinon, P.; Perez, A.; Gierak, J.; Faini, G.; Bourhis, E.; Mailly, D. Gold Nanoparticle Arrays on Graphite Surfaces. *Appl. Surf. Sci.* **2004**, *226*, 173–177.
- (148) Melinon, P.; Hannour, A.; Bardotti, L.; Prevel, B.; Gierak, J.; Bourhis, E.; Faini, G.; Canut, B. Ion Beam Nanopatterning in Graphite: Characterization of Single Extended Defects. *Nanotechnology* **2008**, *19*, 235305.
- (149) Luo, S. N.; Kono, A.; Nouchi, N.; Shoji, F. Effective Creation of Oxygen Vacancies as an Electron Carrier Source in Tin-Doped Indium Oxide Films by Plasma Sputtering. *J. Appl. Phys.* **2006**, *100*, 113701.
- (150) Lang, N. D.; Kohn, W. Theory of Metal-Surfaces - Induced Surface Charge and Image Potential. *Phys. Rev. B: Condens. Matter* **1973**, *7*, 3541–3550.
- (151) Laskin, J.; Wang, P.; Hadjar, O.; Futrell, J. H.; Alvarez, J.; Cooks, Z. G. Charge Retention by Peptide Ions Soft-Landed Onto Self-Assembled Monolayer Surfaces. *Int. J. Mass Spectrom.* **2007**, *265*, 237–243.
- (152) Hadjar, O.; Wang, P.; Futrell, J. H.; Laskin, J. Effect of the Surface on Charge Reduction and Desorption Kinetics of Soft Landed Peptide Ions. *J. Am. Soc. Mass Spectrom.* **2009**, *20*, 901–906.
- (153) Pflaum, J.; Bracco, G.; Schreiber, F.; Colorado, R.; Shmakova, O. E.; Lee, T. R.; Scoles, G.; Kahn, A. Structure and Electronic Properties of CH₃- and CF₃-Terminated Alkanethiol Monolayers on Au(111): A Scanning Tunneling Microscopy, Surface X-Ray and Helium Scattering Study. *Surf. Sci.* **2002**, *498*, 89–104.
- (154) Alloway, D. M.; Hofmann, M.; Smith, D. L.; Gruhn, N. E.; Graham, A. L.; Colorado, R.; Wysocki, V. H.; Lee, T. R.; Lee, P. A.; Armstrong, N. R. Interface Dipoles Arising from Self-Assembled Monolayers on Gold: Uv-Photoemission Studies of Alkanethiols and Partially Fluorinated Alkanethiols. *J. Phys. Chem. B* **2003**, *107*, 11690–11699.
- (155) Love, J. C.; Estroff, L. A.; Kriebel, J. K.; Nuzzo, R. G.; Whitesides, G. M. Self-Assembled Monolayers of Thiolates on Metals as a Form of Nanotechnology. *Chem. Rev.* **2005**, *105*, 1103–1169.
- (156) Waters, T.; Huang, X.; Wang, X. B.; Woo, H. K.; O'Hair, R. A. J.; Wedd, A. G.; Wang, L. S. Photoelectron Spectroscopy of Free Multiply Charged Keggin Anions Alpha-[Pm₁₂O₄₀]³⁻ (M = Mo, W) in the Gas Phase. *J. Phys. Chem. A* **2006**, *110*, 10737–10741.
- (157) Gilb, S.; Weis, P.; Furche, F.; Ahlrichs, R.; Kappes, M. M. Structures of Small Gold Cluster Cations (Au_n⁺, N < 14): Ion Mobility Measurements Versus Density Functional Calculations. *J. Chem. Phys.* **2002**, *116*, 4094–4101.
- (158) Fielicke, A.; von Helden, G.; Meijer, G.; Pedersen, D. B.; Simard, B.; Rayner, D. M. Gold Cluster Carbonyls: Saturated Adsorption of Co on Gold Cluster Cations, Vibrational Spectroscopy, and Implications for Their Structures. *J. Am. Chem. Soc.* **2005**, *127*, 8416–8423.
- (159) Fielicke, A.; von Helden, G.; Meijer, G.; Simard, B.; Rayner, D. M. Gold Cluster Carbonyls: Vibrational Spectroscopy of the Anions and the Effects of Cluster Size, Charge, and Coverage on the Co Stretching Frequency. *J. Phys. Chem. B* **2005**, *109*, 23935–23940.
- (160) Burgel, C.; Reilly, N. M.; Johnson, G. E.; Mitric, R.; Kimble, M. L.; Castleman, A. W.; Bonacic-Koutecky, V. Influence of Charge State on the Mechanism of Co Oxidation on Gold Clusters. *J. Am. Chem. Soc.* **2008**, *130*, 1694–1698.
- (161) Johnson, G. E.; Reilly, N. M.; Tyo, E. C.; Castleman, A. W. Gas-Phase Reactivity of Gold Oxide Cluster Cations with Co. *J. Phys. Chem. C* **2008**, *112*, 9730–9736.
- (162) Freund, H. J.; Pacchioni, G. Oxide Ultra-Thin Films on Metals: New Materials for the Design of Supported Metal Catalysts. *Chem. Soc. Rev.* **2008**, *37*, 2224–2242.
- (163) Shao, X.; Prada, S.; Giordano, L.; Pacchioni, G.; Nilus, N.; Freund, H. J. Tailoring the Shape of Metal Ad-Particles by Doping the Oxide Support. *Angew. Chem., Int. Ed.* **2011**, *50*, 11525–11527.
- (164) Fampiou, I.; Ramasubramaniam, A. Influence of Support Effects on Co Oxidation Kinetics on Co-Saturated Graphene-Supported Pt₁₃ Nanoclusters. *J. Phys. Chem. C* **2015**, *119*, 8703–8710.
- (165) Bonanni, S.; Ait-Mansour, K.; Harbich, W.; Brune, H. Effect of the TiO₂ Reduction State on the Catalytic Co Oxidation on Deposited Size-Selected Pt Clusters. *J. Am. Chem. Soc.* **2012**, *134*, 3445–3450.
- (166) Zhdanov, V. P.; Schweinberger, F. F.; Heiz, U.; Langhammer, C. Ostwald Ripening of Supported Pt Nanoclusters with Initial Size-Selected Distributions. *Chem. Phys. Lett.* **2015**, *631*, 21–25.
- (167) Wettergren, K.; Schweinberger, F. F.; Deiana, D.; Ridge, C. J.; Crampton, A. S.; Rotzer, M. D.; Hansen, T. W.; Zhdanov, V. P.; Heiz, U.; Langhammer, C. High Sintering Resistance of Size-Selected Platinum Cluster Catalysts by Suppressed Ostwald Ripening. *Nano Lett.* **2014**, *14*, 5803–5809.
- (168) Fukamori, Y.; Konig, M.; Yoon, B.; Wang, B.; Esch, F.; Heiz, U.; Landman, U. Fundamental Insight Into the Substrate-Dependent Ripening of Monodisperse Clusters. *ChemCatChem* **2013**, *5*, 3330–3341.
- (169) Bonanni, S.; Ait-Mansour, K.; Harbich, W.; Brune, H. Reaction-Induced Cluster Ripening and Initial Size-Dependent Reaction Rates for Co Oxidation on Pt-N/TiO₂(110)-(1 × 1). *J. Am. Chem. Soc.* **2014**, *136*, 8702–8707.
- (170) Bernhardt, T. M. Gas-Phase Kinetics and Catalytic Reactions of Small Silver and Gold Clusters. *Int. J. Mass Spectrom.* **2005**, *243*, 1–29.
- (171) Li, L.; Gao, Y.; Li, H.; Zhao, Y.; Pei, Y.; Chen, Z. F.; Zeng, X. C. Co Oxidation on TiO₂ (110) Supported Subnanometer Gold Clusters: Size and Shape Effects. *J. Am. Chem. Soc.* **2013**, *135*, 19336–19346.
- (172) Heiz, U. Size-Selected, Supported Clusters: The Interaction of Carbon Monoxide with Nickel Clusters. *Appl. Phys. A: Mater. Sci. Process.* **1998**, *67*, 621–626.
- (173) Sanchez, A.; Abbet, S.; Heiz, U.; Schneider, W. D.; Hakkinen, H.; Barnett, R. N.; Landman, U. When Gold Is Not Noble: Nanoscale Gold Catalysts. *J. Phys. Chem. A* **1999**, *103*, 9573–9578.
- (174) Habibpour, V.; Yin, C. R.; Kwon, G.; Vajda, S.; Palmer, R. E. Catalytic Oxidation of Cyclohexane by Size-Selected Palladium Clusters Pinned on Graphite. *J. Exp. Nanosci.* **2013**, *8*, 993–1003.
- (175) Lei, Y.; Mehmood, F.; Lee, S.; Greeley, J.; Lee, B.; Seifert, S.; Winans, R. E.; Elam, J. W.; Meyer, R. J.; Redfern, P. C.; et al. Increased

Silver Activity for Direct Propylene Epoxidation Via Subnanometer Size Effects. *Science* **2010**, *328*, 224–228.

(176) Lee, S.; Molina, L. M.; Lopez, M. J.; Alonso, J. A.; Hammer, B.; Lee, B.; Seifert, S.; Winans, R. E.; Elam, J. W.; Pellin, M. J.; et al. Selective Propene Epoxidation on Immobilized Au_{6–10} Clusters: The Effect of Hydrogen and Water on Activity and Selectivity. *Angew. Chem., Int. Ed.* **2009**, *48*, 1467–1471.

(177) Kunz, S.; Hartl, K.; Nesselberger, M.; Schweinberger, F. F.; Kwon, G.; Hanzlik, M.; Mayrhofer, K. J. J.; Heiz, U.; Arenz, M. Size-Selected Clusters as Heterogeneous Model Catalysts Under Applied Reaction Conditions. *Phys. Chem. Chem. Phys.* **2010**, *12*, 10288–10291.

(178) Hernandez-Fernandez, P.; Masini, F.; McCarthy, D. N.; Strebel, C. E.; Friebel, D.; Deiana, D.; Malacrida, P.; Nierhoff, A.; Bodin, A.; Wise, A. M.; et al. Mass-Selected Nanoparticles of Pt_x as Model Catalysts for Oxygen Electroreduction. *Nat. Chem.* **2014**, *6*, 732–738.

(179) Johnson, G. E.; Moser, T.; Engelhard, M.; Browning, N. D.; Laskin, J. Soft Landing of Reactively Sputtered Ta Nanoparticles for Electrocatalytic O₂ Reduction. *J. Chem. Phys.* **2016**, submitted.

(180) Johnson, G. E.; Wang, C.; Priest, T.; Laskin, J. Monodisperse Au₁₁ Clusters Prepared by Soft Landing of Mass Selected Ions. *Anal. Chem.* **2011**, *83*, 8069–8072.

(181) Li, G.; Jiang, D. E.; Liu, C.; Yu, C. L.; Jin, R. C. Oxide-Supported Atomically Precise Gold Nanocluster for Catalyzing Sonogashira Cross-Coupling. *J. Catal.* **2013**, *306*, 177–183.

(182) Herzing, A. A.; Kiely, C. J.; Carley, A. F.; Landon, P.; Hutchings, G. J. Identification of Active Gold Nanoclusters on Iron Oxide Supports for Co Oxidation. *Science* **2008**, *321*, 1331–1335.

(183) Turner, M.; Golovko, V. B.; Vaughan, O. P. H.; Abdulkhan, P.; Berenguer-Murcia, A.; Tikhov, M. S.; Johnson, B. F. G.; Lambert, R. M. Selective Oxidation with Dioxygen by Gold Nanoparticle Catalysts Derived from 55-Atom Clusters. *Nature* **2008**, *454*, 981–983.

(184) Yao, H. Optically Active Gold Nanoclusters. *Curr. Nanosci.* **2008**, *4*, 92–97.

(185) Perez, A.; Melinon, P.; Dupuis, V.; Bardotti, L.; Masenelli, B.; Tournus, F.; Prevel, B.; Tuaille-Combes, J.; Bernstein, E.; Tamion, A.; et al. Functional Nanostructures from Clusters. *Int. J. Nanotechnol.* **2010**, *7*, 523–574.

(186) Kauffman, D. R.; Alfonso, D.; Matranga, C.; Ohodnicki, P.; Deng, X. Y.; Siva, R. C.; Zeng, C. J.; Jin, R. C. Probing Active Site Chemistry with Differently Charged Au₂₅^q Nanoclusters (Q = -1, 0, +1). *Chem. Sci.* **2014**, *5*, 3151–3157.

(187) Yang, H. Y.; Wang, Y.; Lei, J.; Shi, L.; Wu, X. H.; Mäkinen, V.; Lin, S. C.; Tang, Z. C.; He, J.; Hakkinen, H.; et al. Ligand-Stabilized Au₁₃Cu_x (X = 2, 4, 8) Bimetallic Nanoclusters: Ligand Engineering to Control the Exposure of Metal Sites. *J. Am. Chem. Soc.* **2013**, *135*, 9568–9571.

(188) Lopez-Sanchez, J. A.; Dimitratos, N.; Hammond, C.; Brett, G. L.; Kesavan, L.; White, S.; Miedziak, P.; Tiruvalam, R.; Jenkins, R. L.; Carley, A. F.; et al. Facile Removal of Stabilizer-Ligands from Supported Gold Nanoparticles. *Nat. Chem.* **2011**, *3*, 551–556.

(189) Kousksou, T.; Bruel, P.; Jamil, A.; El Rhafiki, T.; Zeraoui, Y. Energy Storage: Applications and Challenges. *Sol. Energy Mater. Sol. Cells* **2014**, *120*, 59–80.

(190) Goodenough, J. B. Electrochemical Energy Storage in a Sustainable Modern Society. *Energy Environ. Sci.* **2014**, *7*, 14–18.

(191) Simon, P.; Gogotsi, Y.; Dunn, B. Where Do Batteries End and Supercapacitors Begin? *Science* **2014**, *343*, 1210–1211.

(192) Sathiyaa, M.; Prakash, A. S.; Ramesha, K.; Tarascon, J. M.; Shukla, A. K. V₂O₅-Anchored Carbon Nanotubes for Enhanced Electrochemical Energy Storage. *J. Am. Chem. Soc.* **2011**, *133*, 16291–16299.

(193) Shen, P. K.; Wang, C.-Y.; Jiang, S. P.; Sun, X.; Zhang, J. *Electrochemical Energy: Advanced Materials and Technologies*; CRC Press: New York, 2015.

(194) Xia, H.; Shirley Meng, Y.; Yuan, G.; Cui, C.; Lu, L. A Symmetric RuO₂/RuO₂ Supercapacitor Operating at 1.6 V by Using a

Neutral Aqueous Electrolyte. *Electrochem. Solid-State Lett.* **2012**, *15*, A60–A60.

(195) Lang, X.; Hirata, A.; Fujita, T.; Chen, M. Nanoporous Metal/Oxide Hybrid Electrodes for Electrochemical Supercapacitors. *Nat. Nanotechnol.* **2011**, *6*, 232–236.

(196) Vlad, A.; Singh, N.; Rolland, J.; Melinte, S.; Ajayan, P. M.; Gohy, J. F. Hybrid Supercapacitor-Battery Materials for Fast Electrochemical Charge Storage. *Sci. Rep.* **2014**, *4*, 4315–4315.

(197) Ghosh, D.; Giri, S.; Mandal, M.; Das, C. K. High Performance Supercapacitor Electrode Material Based on Vertically Aligned Pani Grown on Reduced Graphene Oxide/Ni(OH)₂ Hybrid Composite. *RSC Adv.* **2014**, *4*, 26094–26101.

(198) Suárez-Guevara, J.; Ruiz, V.; Gomez-Romero, P. Hybrid Energy Storage: High Voltage Aqueous Supercapacitors Based on Activated Carbon-Phosphotungstate Hybrid Materials. *J. Mater. Chem. A* **2014**, *2*, 1014–1014.

(199) Cuentas-Gallegos, A. K.; Martínez-Rosales, R.; Baibarac, M.; Gómez-Romero, P.; Rincón, M. E. Electrochemical Supercapacitors Based on Novel Hybrid Materials Made of Carbon Nanotubes and Polyoxometalates. *Electrochem. Commun.* **2007**, *9*, 2088–2092.

(200) Genovese, M.; Lian, K. Polyoxometalate Modified Inorganic–Organic Nanocomposite Materials for Energy Storage Applications: A Review. *Curr. Opin. Solid State Mater. Sci.* **2015**, *19*, 126–137.

(201) Wang, H.; Hamanaka, S.; Nishimoto, Y.; Irle, S.; Yokoyama, T.; Yoshikawa, H.; Awaga, K. In Operando X-Ray Absorption Fine Structure Studies of Polyoxometalate Molecular Cluster Batteries: Polyoxometalates as Electron Sponges. *J. Am. Chem. Soc.* **2012**, *134*, 4918–4924.

(202) Garrigue, P.; Delville, M.-H.; Labrugere, C.; Cloutet, E.; Kulesza, P.; Morand, J. P.; Kuhn, A. Top - Down Approach for the Preparation of Colloidal Carbon Nanoparticles. *Chem. Mater.* **2004**, *16*, 2984–2986.

(203) Rong, C.; Anson, F. C. Spontaneous Adsorption of Heteropolytungstates and Heteropolymolybdates on the Surfaces of Solid Electrodes and the Electrocatalytic Activity of the Adsorbed Anions. *Inorg. Chim. Acta* **1996**, *242*, 11–16.

(204) López, X.; Fernández, J. A.; Poblet, J. M. Redox Properties of Polyoxometalates: New Insights on the Anion Charge Effect. *Dalton Transactions* **2006**, 1162–1167.

(205) von Weber, A.; Baxter, E. T.; White, H. S.; Anderson, S. L. Cluster Size Controls Branching Between Water and Hydrogen Peroxide Production in Electrochemical Oxygen Reduction at Ptn/Ito. *J. Phys. Chem. C* **2015**, *119*, 11160–11170.

(206) Proch, S.; Wirth, M.; White, H. S.; Anderson, S. L. Strong Effects of Cluster Size and Air Exposure on Oxygen Reduction and Carbon Oxidation Electrocatalysis by Size-Selected Pt_n (N ≤ 11) on Glassy Carbon Electrodes. *J. Am. Chem. Soc.* **2013**, *135*, 3073–3086.

(207) Penner, R. M.; Gogotsi, Y. The Rising and Receding Fortunes of Electrochemists. *ACS Nano* **2016**, *10*, 3875–3876.

(208) Laaksonen, T.; Ruiz, V.; Liljeroth, P.; Quinn, B. M. Quantised Charging of Monolayer-Protected Nanoparticles. *Chem. Soc. Rev.* **2008**, *37*, 1836–1846.

(209) Mertens, S. F. L.; Vollmer, C.; Held, A.; Aguirre, M. H.; Walter, M.; Janiak, C.; Wandlowski, T. "Ligand-Free" Cluster Quantized Charging in an Ionic Liquid. *Angew. Chem., Int. Ed.* **2011**, *50*, 9735–9738.

(210) Eckermann, A. L.; Feld, D. J.; Shaw, J. A.; Meade, T. J. Electrochemistry of Redox-Active Self-Assembled Monolayers. *Coord. Chem. Rev.* **2010**, *254*, 1769–1802.

(211) Lin, P.; Yan, F. Organic Thin-Film Transistors for Chemical and Biological Sensing. *Adv. Mater.* **2012**, *24*, 34–51.

(212) Halik, M.; Hirsch, A. The Potential of Molecular Self-Assembled Monolayers in Organic Electronic Devices. *Adv. Mater.* **2011**, *23*, 2689–2695.

(213) Smith, R. K.; Nanayakkara, S. U.; Woehle, G. H.; Pearl, T. P.; Blake, M. M.; Hutchison, J. E.; Weiss, P. S. Spectral Diffusion in the Tunneling Spectra of Ligand-Stabilized Undecagold Clusters. *J. Am. Chem. Soc.* **2006**, *128*, 9266–9267.

(214) Chu, C. W.; Na, J. S.; Parsons, G. N. Conductivity in Alkylamine/Gold and Alkanethiol/Gold Molecular Junctions Measured in Molecule/Nanoparticle/Molecule Bridges and Conducting Probe Structures. *J. Am. Chem. Soc.* **2007**, *129*, 2287–2296.

(215) Seidel, Y. E.; Schneider, A.; Jusys, Z.; Wickman, B.; Kasemo, B.; Behm, R. J. Mesoscopic Mass Transport Effects in Electrocatalytic Processes. *Faraday Discuss.* **2009**, *140*, 167–184.

(216) Kleijn, S. E.; Lai, S. C.; Koper, M. T.; Unwin, P. R. Electrochemistry of Nanoparticles. *Angew. Chem., Int. Ed.* **2014**, *53*, 3558–86.

(217) Crabtree, G. W.; Sarrao, J. L. Opportunities for Mesoscale Science. *MRS Bull.* **2012**, *37*, 1079–1088.